C.P. No. 1097

C.P. No 1097

MINISTRY OF TECHNOLOGY

AERONAUTICAL RESEARCH COUNCIL

CURRENT PAPERS

Low-Speed Wind-Tunnel Measurements of the Oscillatory Lateral Stability Derivatives for a Model of a Slender Aircraft (HP 115) including the Effects of Frequency Parameter

by

J. S Thompson, R A Fail and J V Inglesby

Aerodynamics Dept., R.A.E, Bedford

LONDON HER MAJESTY'S STATIONERY OFFICE

1970

PRICE *13s 0d* [*65p*] NET

C.P. No. 1097*
February 1969

U.D.C. 533.693.3 : 533.6.013.413 : 533.6.013.417 : 533.6.013.42

LOW-SPEED WIND-TUNNEL MEASUREMENTS OF THE OSCILLATORY LATERAL STABILITY DERIVATIVES FOR A MODEL OF A SLENDER AIRCRAFT (HP 115) INCLUDING THE EFFECTS OF FREQUENCY PARAMETER

by

J. S. Thompson

R. A. Fail

J. V. Inglesby

Aerodynamics Department, R.A.E., Bedford

SUMMARY

Low-speed tunnel tests on a model of the HP 115 aircraft have provided a complete set of lateral derivatives for a range of frequency parameters. Over a range appropriate to full scale flight, the effects of frequency parameter are small, but for very high values there is a marked reduction in the derivatives n_p, y_p and ℓ_v. Some information is included on the derivatives $n_{\dot{v}}$, $y_{\dot{v}}$ and $\ell_{\dot{v}}$, and there is evidence that the virtual inertias are about the same wind-on and wind-off.

The Paper also describes some recent improvements in technique.

*Replaces R.A.E. Technical Report 69018 - A.R.C. 31289

CONTENTS

1 INTRODUCTION

Earlier analysis of the dutch roll behaviour of the HP 115 slender wing research aircraft had indicated a strong dependence of the stability of this lateral mode on what are usually considered secondary aerodynamic derivatives and that theoretical methods for their prediction were completely inadequate. Oscillatory wind tunnel tests were therefore made on a model of this aircraft on a rig developed at R.A.E. Bedford as described in Ref.1. Although these tests were generally successful in providing a complete set of lateral derivatives, they still did not lead to perfect agreement with flight results. It was thought that the discrepancy could possibly be due to the fact that the rolling frequency in the wind tunnel was much higher than that appropriate to represent the frequency parameter $\nu(= \omega c_o/V)$ of the relevant rigid body mode of the full scale aircraft. It was decided therefore to investigate the effects of frequency parameter on the derivatives. particularly to find out whether it was necessary to reduce the rolling frequency for routine testing in the 13ft × 9ft tunnel

The frequency could not easily be reduced and significantly higher speeds were not available in the 13ft × 9ft tunnel The first series of tests described in the present report was therefore made in the 8ft × 8ft tunnel at speeds from 100 ft/sec to 300 ft/sec the upper limit being chosen to avoid Mach number effects There was reason to suppose that the steady aerodynamic loads might affect the characteristics of the support system and most of the tests were therefore made at a constant value of $\frac{1}{2} \rho V^2$ The results of these tests showed that some of the derivatives (particularly n_p and y_p) varied markedly with frequency parameter. Attention was therefore concentrated on reducing the rolling frequency and it was found possible to achieve this by a modification to the spring unit. A second series of tests was then made in the 13ft × 9ft tunnel, mainly to try out the modified spring unit. In these tests an unforeseen difficulty appeared; with the lower natural frequency in roll the sideslipping mode became negatively damped over a large part of the incidence range and this had an adverse effect on the quality of the results (see Appendix B). For future testing, a range of spring units (with differing roll stiffnesses) is being made. By a suitable choice of spring unit and more careful design of models it is hoped that reasonably representative values of the frequency parameter will be obtained without encountering unsatisfactory modes of oscillation.

The tests described above have provided a complete set of lateral derivatives for the HP 115 A comprehensive series of flight tests has been made on the full scale aircraft, and this should permit detailed comparison with the results presented here The results of a preliminary analysis of the flight data are given in Ref.2, but these were derived by using assumed values for n_p and the present results show these assumptions to have been seriously in error. Using the present wind tunnel data, the flight results have now been reanalysed and have led to virtually perfect agreement. It is particularly noteworthy that only by making proper allowance for the frequency dependence of the derivative n_p as revealed by the tunnel tests reported here was this agreement obtained. An account of this work will be given in a later report.

2 NOTATION

2.1 List of symbols

b	wing span (ft)
C_m	pitching moment coefficient, $M/\frac{1}{2}\rho V^2 S c_o$
C_X	axial force coefficient, $X/\frac{1}{2}\rho V^2 S$
C_Z	normal force coefficient, $Z/\frac{1}{2}\rho V^2 S$
c_o	wing centre line chord (ft)
D	displacement matrix
e	aft movement of reference axis (ft)
F	force matrix
g	acceleration due to gravity (ft/sec^2)
H	tunnel pressure, inches of mercury
h	distance of axis forward of sting root (ft)
I_{XX}	rolling moment of inertia (slug ft^2)
I_{ZZ}	yawing moment of inertia (slug ft^2)
I_1 to I_{10}	integrals defined by equations (A-8) to (A-11) and (A-14) to (A-19)
K_1 to K_4	constants defined by equations (A-20)
L	rolling moment (lb ft)
ℓ (with suffix)	nondimensional rolling moment derivative
M	pitching moment (lb ft)
m	mass (slug)
N	yawing moment (lb ft)
n (with suffix)	nondimensional yawing moment derivative
P	defined in equations (A-21)
p	angular velocity in roll (rad/sec)
R	Reynolds number based on c_o
r	angular velocity in yaw (rad/sec)
S	wing area (ft^2)
V	free stream velocity (ft/sec)
v	nondimensional sideslip, $\dot{y}/V$ (angle of sideslip)

X	axial force (lb)
x	distance forward of sting root (ft)
$\bar{x}$	distance of model cg ahead of reference axis (ft)
Y	side force (lb)
y	sideways displacement (ft)
y (with suffix)	nondimensional side force derivative
Z	normal force (lb)
α	angle of incidence
Λ, Λ_M, Λ_Z	flexibility matrices defined by equations (A-1) and (A-2)
λ	bending flexibility per unit length
μ	torsional flexibility per unit length
ν	frequency parameter, $\omega c_o/V$
ρ	air density (slug/ft^3)
ϕ	angular displacement in roll (rad)
ψ	angular displacement in yaw (rad)
ω	circular frequency (rad/sec)

Suffixes

p, r, v, y, ϕ, ψ	denote derivatives with respect to these variables
1	denotes increments due to steady Z and M

2.2 Axes

The principal results of these tests are given in body axes notation, with independent variables v, p and r. In the reduction of the measurements a system of earth axes is used, fixed in the mean position of the oscillating model, and in this system the model displacements are denoted by ψ, y and ϕ. Forces and moments are always referred to body axis.

2.3 Derivatives

The derivatives as measured include the characteristics of the spring unit, which are allowed for by subtracting wind-off values normally measured at the same tunnel pressure (but see section 5.3). In addition certain other corrections have to be applied, to allow for the effects of the steady aerodynamic normal force and pitching moment (see section 3).

The Aerodynamic derivatives so obtained (such as N_ψ and $N_{\dot\psi}$) are in terms of forces and moments referred to body axes, and motions referred to earth axes.

Finally, the aerodynamic derivatives have to be expressed in terms of the motion parameters r, p and v. It is a common limitation of this type of wind tunnel testing that as a result of the kinematic constraint on the model these variables cannot generally be separated, and the results can be expressed only as combinations. The relationship between the directly measured tunnel derivatives ($N_{\dot\psi}$, $N_{\dot\phi}$ etc., or nondimensionally $n_{\dot\psi}$, $n_{\dot\phi}$ etc.) and the corresponding body axis derivatives (n_r, $n_{\dot v}$ etc.) are given by the following equations:-

$$n_r - n_{\dot v}\cos\alpha = n_{\dot\psi} = N_{\dot\psi}/(\tfrac{1}{2}\rho V S c_o^2)$$

$$n_p + n_{\dot v}\sin\alpha = n_{\dot\phi} = N_{\dot\phi}/(\tfrac{1}{2}\rho V S c_o^2)$$

$$y_r - y_{\dot v}\cos\alpha = y_{\dot\psi} = Y_{\dot\psi}/(\tfrac{1}{2}\rho V S c_o)$$

$$y_p + y_{\dot v}\sin\alpha = y_{\dot\phi} = Y_{\dot\phi}/(\tfrac{1}{2}\rho V S c_o)$$

$$\ell_r - \ell_{\dot v}\cos\alpha = \ell_{\dot\psi} = L_{\dot\psi}/(\tfrac{1}{2}\rho V S c_o^2)$$

$$\ell_p + \ell_{\dot v}\sin\alpha = \ell_{\dot\phi} = L_{\dot\phi}/(\tfrac{1}{2}\rho V S c_o^2)$$

$$-n_v\cos\alpha = n_\psi = N_\psi/(\tfrac{1}{2}\rho V^2 S c_o)$$

$$n_v = n_{\dot y} = N_{\dot y}/(\tfrac{1}{2}\rho V S c_o)$$

$$n_v\sin\alpha = n_\phi = N_\phi/(\tfrac{1}{2}\rho V^2 S c_o)$$

$$-y_v\cos\alpha = y_\psi = Y_\psi/(\tfrac{1}{2}\rho V^2 S)$$

$$y_v = y_{\dot y} = Y_{\dot y}/(\tfrac{1}{2}\rho V S)$$

$$y_v\sin\alpha = y_\phi = y_\phi/(\tfrac{1}{2}\rho V^2 S)$$

$$-\ell_v \cos\alpha = \ell_\psi = L_\psi/(\tfrac{1}{2}\rho V^2 S c_o)$$

$$\ell_v = \ell_{\dot{y}} = L_{\dot{y}}/(\tfrac{1}{2}\rho V S c_o)$$

$$\ell_v \sin\alpha = \ell_\phi = L_\phi/(\tfrac{1}{2}\rho V^2 S c_o)$$

(These three derivatives should all be zero)

$$\left\{\begin{aligned} n_y &= N_y/(\tfrac{1}{2}\rho V^2 S) \\ y_y &= Y_y/(\tfrac{1}{2}\rho V^2 S/c_o) \\ \ell_y &= L_y/(\tfrac{1}{2}\rho V^2 S) \end{aligned}\right.$$

$$n_{\dot{v}} = n_{\ddot{y}} = N_{\ddot{y}}/(\tfrac{1}{2}\rho S c_o^2)$$

$$y_{\dot{v}} = y_{\ddot{y}} = Y_{\ddot{y}}/(\tfrac{1}{2}\rho S c_o)$$

$$\ell_{\dot{v}} = \ell_{\ddot{y}} = L_{\ddot{y}}/(\tfrac{1}{2}\rho S c_o^2)$$

(These two derivatives represent virtual inertias)

$$\left\{\begin{aligned} n_{\ddot{\psi}} &= N_{\ddot{\psi}}/(\tfrac{1}{2}\rho S c_o^3) \\ \ell_{\ddot{\phi}} &= L_{\ddot{\phi}}/(\tfrac{1}{2}\rho S c_o^3) \end{aligned}\right.$$

3 CORRECTIONS FOR THE EFFECTS OF STEADY LOADS

The application of a steady load to a model on a spring unit may introduce cross-stiffnesses.

Consider, for example, the effect of aerodynamic normal force. In our spring units the roll flexibility is nearly all forward of the sideslip flexibility, so that the normal force, rolling with the model, produces a sideways displacement proportional to the roll angle. Thus the presence of the normal force introduces a cross-stiffness which in the analysis of the results is included in the aerodynamic derivative Y_ϕ. For our purpose, however, it is equivalent to a mechanical cross-stiffness, and must therefore be treated as a correction to be subtracted from the measured aerodynamic derivative.

The magnitudes of this and other similar corrections could be determined from static loading tests, with suitable measuring equipment, but we have found it satisfactory to calculate them from the geometry of the spring units, as described in Appendix A.

The following equations give in nondimensional form the values of the corrections due to the steady normal force and pitching moment. The effects of axial force are insignificant, and no steady lateral loads have been applied in these tests. The suffix 1 denotes a correction to be subtracted from the measured value.

For the original spring unit:-

$$(n_\phi)_1 = 0.005\ C_Z + 0.391\ C_m \tag{3-1}$$

$$(y_\phi)_1 = -0.951\ C_Z + 1.435\ C_m \tag{3-2}$$

$$(\ell_\psi)_1 = 0.005\ C_Z - 0.609\ C_m \tag{3-3}$$

$$(\ell_y)_1 = 0.049\ C_Z + 1.435\ C_m \tag{3-4}$$

and for the modified spring unit:-

$$(n_\phi)_1 = 0.003\ C_Z + 0.425\ C_m \tag{3-5}$$

$$(y_\phi)_1 = -0.973\ C_Z + 1.485\ C_m \tag{3-6}$$

$$(\ell_\psi)_1 = 0.003\ C_Z - 0.575\ C_m \tag{3-7}$$

$$(\ell_y)_1 = 0.027\ C_Z + 1.485\ C_m\ . \tag{3-8}$$

(It may be noted that in each case there are only four independent constants.)

The largest corrections arise in the case of the derivative y_ϕ, which should be identical with $y_v \sin\alpha$. The order of magnitude of this is illustrated in Fig.22. The lower curve gives the values of $y_v \sin\alpha$ obtained from yawing tests, and by adding to this the calculated correction defined by equation (3-2) we obtain the upper curve, which represents the values of y_ϕ that one would expect to measure. The actual measured values, shown by the separate points, agree quite well. The corrected values of y_ϕ, plotted as $y_v \sin\alpha$ in Fig.19, show a good deal of scatter, which is to be expected when such large corrections have been applied, but there are no systematic discrepancies.

Similar corrections (but with different numerical constants) are needed for the effects of gravitational forces on the model, but these are independent of aerodynamic loads and can be eliminated by subtracting wind-off datums at the same incidence.

There is another gravitational effect, of a somewhat analogous kind, for which a correction has to be applied. When the model at an incidence α is subject to yaw and roll displacements ψ and ϕ respectively, a sideslip accelerometer in the model will give a reading

$$\ddot{y} = - g (\psi \sin \alpha + \phi \cos \alpha)$$

which must be deducted from the measured $\ddot{y}$ before it is used in the equations of motion. This is most conveniently done by expressing the correction in the form

$$\ddot{y} = \frac{g}{\omega^2} (\ddot{\psi} \sin \alpha + \ddot{\phi} \cos \alpha) \quad .$$

All the corrections described in this section have been applied to the measured values before using the axis conversion equations given at the end of section 2.

4 DESCRIPTION OF TESTS

4.1 Model and test conditions

A sketch of the model is given in Fig.1 and the main dimensions in Table 1. The engine air intake was closed and faired over, and a certain amount of distortion at the rear of the model was necessary to accommodate the sting, as shown by the shaded areas in Fig.1. No control surfaces were represented and no arrangements were made to fix transition.

Full details of the various test conditions are given in Table 2.

The ranges of the frequency parameters are shown diagrammatically in Fig.3. In the tests with the modified spring unit, the values of the frequency parameter in the rolling mode were still too high. This was partly because of the limited speed of the 13ft by 9ft tunnel (compared with the 8ft by 8ft) and partly because at high incidence the aerodynamic roll stiffness $(\ell_v \sin \alpha)$

makes a significant contribution to the total stiffness and raises the natural frequency in roll.

4.2 Brief account of method

The method of test was basically as described in Ref.1 and is briefly summarised here. The more important recent improvements are described below in section 4.3.

The model is mounted on a special sting or spring unit (Fig.2) which has a forward spring providing flexibilities in yaw and roll, and a rear spring providing flexibility in sideslip. Oscillations are excited by means of an electromagnetic vibration generator and the motion is measured by means of accelerometers in the model. The system has three modes of oscillation, which are designated yawing, sideslipping and rolling modes. The rolling mode does not generally include much yaw or sideslip, but the yawing oscillation has its axis some distance behind the centre of the forward spring and the sideslipping mode includes a considerable amount of yawing motion. The test procedure is to oscillate the model at or near the natural frequency of each mode in turn (since this is the only way of obtaining reasonable amplitudes with the small excitation force available). Eighteen derivatives are obtained by solving the complete equations of motion, using measured values of the accelerations and excitation forces (as vectors) and frequencies, together with previously determined values of the model inertias. The required aerodynamic derivatives are then obtained as the differences between wind-off and wind-on values of the derivatives; (assuming that the mechanical characteristics of the system are unaffected by the air loads). Since the frequencies are different for the different modes, it is necessary when solving the equations of motion to assume that the derivatives are independent of frequency. This procedure is not strictly correct if the derivatives depend on frequency, but it is considered adequate because, in effect, each derivative is obtained primarily from one of the modes with only small correction terms from the others. The frequency parameters quoted are those for the primary modes for each derivative.

4.3 Recent developments

The following changes have been made in the technique described in Ref.1:

(a) Presentation of results. The main change is to refer the results to body axes (see section 3). The results now include some information on derivatives with respect to $\dot{v}$.

(b) Spring unit. In the course of the tests the spring unit was modified as shown in Fig.2. The modification reduced the natural frequency in roll by a factor of nearly three, while having only a small effect on the natural frequency in yaw, and reducing the permissible normal force and pitching moment by about 35%.

(c) Calibration procedure. Instead of the somewhat complicated procedure of determining the calibration constants by direct calculation of the best values to fit a series of calibration measurements, a simple trial and error method is used which is more satisfactory in several respects. (See Appendix C.)

5 RESULTS

5.1 Presentation

The main results are plotted in Figs.4-21. A summary is given in Table 3 which also serves as an index to the figures. The derivatives with respect to rolling velocity depend on both incidence and frequency parameter, and the frequency parameter itself varies with incidence because of the effect of the aerodynamic roll stiffness, $\ell_v \sin\alpha$, especially in the case of the modified (more flexible) spring. For these derivatives a full set of results is given in Table 4, and the more important points are illustrated in Figs.7, 8 and 9.

The spring unit is fitted with ordinary wire resistance strain gauges forming a five component balance for static measurements. Values of the normal force and pitching moment coefficients and the static lateral derivatives measured with this balance in the 13ft by 9ft tunnel are given in Table 5. These values are used when considering frequency parameter effects ($\nu = 0$ in Figs.11 and 12).

5.2 Damping derivatives

As usual in tests of this kind, the rotary damping derivatives are measured in combination with the derivatives with respect to rate of change of sideslip, $\dot{v}$, as follows:-

$$n_r - n_{\dot{v}} \cos\alpha \qquad \text{(measured as } n_{\dot{\psi}}\text{)}$$

$$n_p + n_{\dot{v}} \sin\alpha \qquad \text{(measured as } n_{\dot{\phi}}\text{)}$$

and similarly for y and ℓ. In the present tests separate value of the $\dot{v}$ derivatives are also obtained, although in practice the results are very scattered. However, it is concluded in section 5.3 that the $\dot{v}$ derivatives are probably small compared with the rotary damping derivatives except in the case of $y_{\dot{v}}$ compared with y_r.

The combined derivatives $(n_r - n_{\dot{v}} \cos \alpha)$, $(y_r - y_{\dot{v}} \cos \alpha)$ and $(\ell_r - \ell_{\dot{v}} \cos \alpha)$ are shown in Figs.4, 5 and 6 respectively. The measurements seem reasonably satisfactory and there is no significant variation with frequency parameter over the range tested (0.36 - 1.02). There is some indication that the 13ft by 9ft tunnel tests (shown by triangles) give smaller values of the yaw damping than the 8ft by 8ft tests (Fig.4), but this is considered more likely to be due to experimental error than to a genuine aerodynamic effect. In all these figures the 13ft by 9ft results show rather more scatter than the 8ft by 8ft results; this is attributed to the slightly less satisfactory support system in the 13ft by 9ft tunnel. In the 8ft by 8ft tests, the scatter is greatest for the lowest values of the frequency parameter, particularly in the case of the circles in Fig.6. This is because the damping forces, which are proportional to ρV, have to be measured in the presence of the main aerodynamic forces which are proportional to ρV^2. At low values of frequency parameter, corresponding to high values of the tunnel speed V, the damping forces are thus a smaller proportion of the total and are more difficult to measure accurately.

For the derivatives $(n_p + n_{\dot{v}} \sin \alpha)$, $(y_p + y_{\dot{v}} \sin \alpha)$ and $(\ell_p + \ell_{\dot{v}} \sin \alpha)$, the values of the frequency parameter were still rather high, even with the more flexible spring unit used in the 13ft by 9ft tunnel tests (see Table 4). The n and y derivatives show large variations with frequency parameter (Figs.7 and 8). There is considerable scatter, but the variations appear to be greatest in the middle of the range of frequency parameter, and it is possible that the curves flatten out at frequency parameters below about 1. The ℓ derivative (Fig.9) shows no evidence of frequency parameter effects.

5.3 Virtual inertias and derivatives with respect to rate of change of sideslip $\dot{v}$

The virtual inertias and $\dot{v}$ derivatives are difficult to measure accurately, and we have not so far made any serious attempt to do so. The present tests, however, have provided some information on these derivatives, mainly because they cover a wide range of frequency parameters. We have not presented the actual values of the derivatives, because they would not be accurate and might be misleading. Instead, we have plotted the measurements from which these derivatives can be deduced as slopes or differences; this makes it easier to assess the significance of the effects and the accuracy with which they can be measured.

The total aerodynamic effects on the model are obtained by subtracting a datum measured in a vacuum. Stiffness derivatives obtained in this way will include virtual inertia effects, since our method of analysis does not distinguish them, and the apparent stiffness N_ψ, for instance, will represent $(N_\psi - \omega^2 N_{\ddot\psi})$, or in nondimensional terms $(n_\psi - \nu^2 n_{\ddot\psi})$. (This relation is not exact because additional terms are introduced by coupling between modes.) By comparing tests at different values of the frequency parameter ν, it is possible to separate the stiffness n_ψ and the virtual inertia $- n_{\ddot\psi}$, making the assumption that both these derivatives are independent of ν.

The most important derivatives of this kind are those with respect to $\dot v$ $(= \ddot y/V)$ because these are associated with the rotary damping derivatives with respect to r (and, to a lesser extent, p). The values of the measured apparent stiffnesses n_y, y_y and ℓ_y are plotted against ν^2 in Fig.10. These derivatives have been referred to vacuum datums, and the values should, ideally, give straight lines passing through zero (since the true stiffnesses are zero) and with slopes roughly equal to the corresponding $\dot v$ derivatives. As an indication of the scale, lines have been drawn on Fig.10 representing certain values of these derivatives.

The plotted points showing the measurements are too scattered to provide much positive information, but in the case of $n_{\dot v}$ and $\ell_{\dot v}$ they are not inconsistent with small values of these derivatives. It is concluded that the derivatives with respect to rate of change of sideslip, $n_{\dot v}$ and $\ell_{\dot v}$, do not make a large contribution to the total damping derivatives $(n_r - n_{\dot v} \cos \alpha)$ and $(\ell_r - \ell_{\dot v} \cos \alpha)$ measured in the yawing mode and shown in Figs.4 and 6. The value of $y_{\dot v}$, however, is not small, and could be as much as -0.1, (the still air value is rather larger than this - see below). This means that $- y_{\dot v} \cos \alpha$ may be the major part of $(y_r - y_{\dot v} \cos \alpha)$ (Fig.5), and that y_r may be comparatively small.

The virtual inertias $n_{\ddot\psi}$ and $\ell_{\ddot\phi}$ are of less importance, but are not without interest. The apparent aerodynamic stiffnesses n_ψ and ℓ_ϕ have each been obtained in two ways: the values in Figs.11a and 12a are referred to wind-off datums at the same pressures as the corresponding wind-on tests, while those in Figs.11b and 12b are referred to vacuum datums. The latter curves show systematic frequency parameter effects which in most cases are practically eliminated when the datum is the wind-off value at the same tunnel pressure. From this it may be concluded that Figs.11a and 12a give the true stiffness derivatives, while Figs.11b and 12b include the effects of appreciable virtual inertias which have about the same values wind-on and wind-off. Fig.12a also shows that ℓ_ϕ $(= \ell_v \sin\alpha)$ has decreased nearly to zero at $\nu = 4$ (which corresponds to a wavelength of only $1\frac{1}{2}$ chords). This result is in good agreement with earlier measurements by Owen. These are described in Ref.3 which also offers an explanation in terms of vortex lag.

The virtual inertias have been determined in still air by comparing the apparent model inertias measured at various tunnel pressures, assuming that the mechanical stiffnesses remain constant and that the aerodynamic stiffnesses are zero.

The three primary inertias obtained in this way are shown in Fig.13, where the slopes of the lines give the virtual inertias. (This virtual mass, of course, applies to lateral tests only; a different value would be measured in heaving motion.) The value of $y_{\ddot{y}}$ is -0.15. As already remarked, this is rather larger than the value deduced from Fig.10 for $y_{\dot{v}}$ (nominally the same derivative) in the wind-on case.

The still air values of $n_{\ddot{\psi}}$ and $\ell_{\ddot{\phi}}$ give the numerical values of the virtual inertias whose existence is indicated by comparisons between Figs.11a and 11b, and 12a and 12b, respectively. These are not large, and, as already mentioned, are excluded from the stiffness derivatives by the method of subtracting wind-off zeros at the same pressure.

The still air values of the six virtual cross-inertias are all too small to measure. The results are not presented, but they show that $n_{\ddot{y}}$ and $\ell_{\ddot{y}}$ are certainly not larger than the extreme values of $n_{\dot{v}}$ and $\ell_{\dot{v}}$ shown on Fig.10; that $n_{\ddot{\phi}}$, $y_{\ddot{\phi}}$ and $\ell_{\ddot{\psi}}$ are too small to have any significant effect on the corresponding stiffness measurements; and that the effect of $y_{\ddot{\psi}}$ on the measurement of y_ψ is not larger than the scatter of the y_ψ readings (shown as y_v in Fig.17).

The above remarks are concerned with the effect of datum pressures on stiffnesses and inertias, but their effect on damping measurements should also be mentioned. In the present tests the still air damping values were always small, and only two showed any consistent pressure effects; ℓ_ϕ and n_ψ both increased with tunnel pressure. In no case was the change large enough to have any significant effect on the aerodynamic results.

5.4 Stiffness derivatives

The derivatives n_v, y_v and ℓ_v are shown in Figs.14-21. Three sets of values can be measured for each of these derivatives, distinguished only by the frequency parameters of the appropriate modes. For example n_ψ $(= - n_v \cos \alpha)$ is measured as a direct stiffness. (The effects of virtual inertia have been largely eliminated by using a wind-off stiffness measured at the same tunnel pressure as described in section 5.3.) The results for n_v $(= - n_\psi/\cos \alpha)$ are shown in Fig.14. The derivative $n_{\dot{y}}$ $(= n_v)$ is measured as a cross-damping; these results are shown in Fig.15. Finally, the derivative n_ϕ $(= n_v \sin \alpha)$ is measured as a cross-stiffness. In this case accurate values of n_v obviously cannot be obtained at small values of α and the results (Fig.16) are mainly of interest as a check.

Similar sets of results are given for the side force derivatives (Figs.17-19) and for the rolling moment derivatives (Figs.20 and 21). Fig.12 shows values of ℓ_ϕ $(= \ell_v \sin \alpha)$, which have been discussed in section 5.3.

Generally there is more scatter in the results obtained from the side-slipping motion than in those obtained from the yawing motion. This is partly because damping measurements are nearly always more difficult to make than stiffness measurements. However, the worst scatter occurs in the 13ft by 9ft tunnel tests (triangular points in Figs.15 and 18) when the results were probably adversely affected by the occurrence of a negatively damped sideslipping mode (see Appendix B).

There is some indication that the 13ft by 9ft tunnel tests give lower values of n_v than the 8ft by 8ft tests (Fig.14), but this is considered more likely to be due to experimental error than to a genuine aerodynamic effect.

Except in the case of ℓ_ϕ (discussed in section 5.3) the effects of frequency parameter on all of these derivatives appear to be small, and the generally satisfactory agreement between these stiffness and damping measurements may be regarded as a check on the reliability of the other damping measurements.

6 CONCLUSIONS

(a) A complete set of low speed lateral derivatives for a model of the HP 115 has been measured over a wide range of frequency parameter, although the lowest values of the rolling frequency parameter that were obtained were higher than those appropriate to the rigid body modes of the full scale aircraft.

(b) For a range of frequency parameter appropriate to full scale flight, the variations of the derivatives are small, but for very high values of the frequency parameter there are marked reductions in the derivatives n_p, y_p and ℓ_v.

(c) The derivatives with respect to rate of change of sideslip, $n_{\dot{v}}$ and $\ell_{\dot{v}}$, could not be measured accurately but there is some indication that they are smaller than n_r and ℓ_r respectively. The derivative $y_{\dot{v}}$, however, is not small and may be larger than y_r.

(d) The primary virtual inertias $-n_{\ddot{\psi}}$ and $-\ell_{\ddot{\phi}}$ are found to be nearly the same wind-on and wind-off.

(e) Certain stiffness derivatives required large corrections for the effects of steady normal force and pitching moment. In particular it is impossible to measure $\ell_{\dot{v}}$ unless the proper corrections have been applied to the stiffness derivative ℓ_y.

Appendix A

CALCULATION OF CORRECTIONS FOR THE EFFECT OF STEADY NORMAL FORCE AND PITCHING MOMENT ON LATERAL STIFFNESS DERIVATIVES

Method

From a knowledge of the dimensions and elastic constants of the sting we first calculate the end displacements ψ, y, ϕ produced by loads N, Y and L applied at the end of the sting. This gives us a 3 by 3 flexibility matrix Λ defined by

$$D = \Lambda F \tag{A-1}$$

where $D = \begin{bmatrix} \psi \\ y \\ \phi \end{bmatrix}$ and $F = \begin{bmatrix} N \\ Y \\ L \end{bmatrix}$

Next we calculate the additional displacements D_1 produced by additional loads Z and M at the end of the sting, applied in the presence of F. This gives two second order flexibilities Λ_Z and Λ_M defined by

$$D_1 = (Z \Lambda_Z + M \Lambda_M) F \quad . \tag{A-2}$$

These additional displacements are those which would be produced by additional forces F_1 given by

$$F_1 = \Lambda^{-1} D_1 \tag{A-3}$$

and from equation (A-1) we also have

$$F = \Lambda^{-1} D \tag{A-4}$$

so that combining equations (A-2), (A-3) and (A-4) gives

$$F_1 = \Lambda^{-1} (Z \Lambda_Z + M \Lambda_M) \Lambda^{-1} D \quad . \tag{A-5}$$

The derivatives with which we are concerned are those defined by the equation

$$F_1 = \begin{bmatrix} 0 & 0 & N_\phi \\ 0 & 0 & Y_\phi \\ L_\psi & L_y & 0 \end{bmatrix} D \qquad \text{(A-6)}$$

and their values can be determined by equating corresponding terms in equations (A-5) and (A-6).

Equation (A-6) includes only four of the possible nine derivatives. This is partly because we have not included the effect of a steady axial force X, which would be very small, and partly because we are dealing with a symmetrical sting with no stiffness coupling between roll and sideslip or yaw.

Calculation of flexibilities

The calculation of the deflections produced by the combined loadings N, Y and L, with and without Z and M, is done by conventional methods. Only the results are given here, in the form of general formulae.

The position of a point on the sting is defined by its distance x forward from the root (earthed) end of the sting. Let λ and μ be the bending and torsional flexibilities per unit length of the sting cross section at the point x. The axis used for moments and displacements is at the position $x = h$, chosen so that the range $x = 0$ to h covers all the flexible part of the sting.

Then the sting flexibility Λ is given by

$$\Lambda = \begin{bmatrix} I_1 & I_2 & 0 \\ I_2 & I_3 & 0 \\ 0 & 0 & I_4 \end{bmatrix} \qquad \text{(A-7)}$$

where

$$I_1 = \int_0^h \lambda \, dx \tag{A-8}$$

$$I_2 = \int_0^h (h - x) \, \lambda \, dx \tag{A-9}$$

$$I_3 = \int_0^h (h - x)^2 \, \lambda \, dx \tag{A-10}$$

$$I_4 = \int_0^h \mu \, dx \quad . \tag{A-11}$$

The second order flexibilities Λ_Z and Λ_M are given by

$$\Lambda_Z = \begin{bmatrix} 0 & 0 & -I_9 \\ 0 & 0 & -I_{10} \\ I_6 & I_7 & 0 \end{bmatrix} \tag{A-12}$$

$$\Lambda_M = \begin{bmatrix} 0 & 0 & I_8 \\ 0 & 0 & I_9 \\ -I_5 & -I_6 & 0 \end{bmatrix} \tag{A-13}$$

where

$$I_5 = \int_0^h \lambda \int_0^x \mu \, dx \, dx \tag{A-14}$$

$$I_6 = \int_0^h (h - x) \, \lambda \int_0^x \mu \, dx \, dx \tag{A-15}$$

$$I_7 = \int_0^h (h - x)^2 \, \lambda \int_0^x \mu \, dx \, dx \tag{A-16}$$

$$I_8 = \int_0^h \mu \int_0^x \lambda \, dx \, dx = I_1 \, I_4 - I_5 \tag{A-17}$$

$$I_9 = \int_0^h \mu \int_0^x (h - x)\, \lambda \, dx\, dx = I_2\, I_4 - I_6 \qquad \text{(A-18)}$$

$$I_{10} = \int_0^h \mu \int_0^x (h - x)^2\, \lambda \, dx\, dx = I_3\, I_4 - I_7 \quad . \qquad \text{(A-19)}$$

Equation (A-5) can now be expressed in terms of the integrals I by using equations (A-7), (A-12) and (A-13), and by comparing the result with equation (A-6) we find that the derivatives can be expressed in terms of four independent constants K, defined by

$$\left.\begin{aligned} N_\phi &= K_4\, Z + (K_2 + 1)\, M \\ Y_\phi &= (K_1 - 1)\, Z + K_3\, M \\ I_\psi &= K_4\, Z + K_2\, M \\ L_y &= K_1\, Z + K_3\, M \end{aligned}\right\} \qquad \text{(A-20)}$$

where the values of K are given by

$$\left.\begin{aligned} K_1 &= (I_1\, I_7 - I_2\, I_6)/P \\ K_2 &= (I_2\, I_6 - I_3\, I_5)/P \\ K_3 &= (I_2\, I_5 - I_1\, I_6)/P \\ K_4 &= (I_3\, I_6 - I_2\, I_7)/P \end{aligned}\right\} \qquad \text{(A-21)}$$

where $P = (I_1\, I_3 - I_2^2)\, I_4$.

Change of axis

These K values apply for the axis at $x = h$ used in the integration. For a reference axis on the model at a distance e aft of this, new values K' have to be used, given by the equations

$$\left.\begin{aligned} K_1' &= K_1 + e\,K_3 \\ K_2' &= K_2 + e\,K_3 \\ K_3' &= K_3 \\ K_4' &= K_4 + e\,(K_1 + K_2) + e^2\,K_3 \end{aligned}\right\} \quad (A\text{-}22)$$

Numerical values

The K values for the stings sketched in Fig.2, with the axis position shown, are given below. (The dimensional quantities K_3 and K_4 have been multiplied and divided by the centre line chord c_o to give the nondimensional numerical constants in section 3.)

	Original	Modified
K_1	0.049	0.027
K_2	-0.609	-0.575
K_3 1/ft	0.287	0.297
K_4 ft	0.023	0.015

For these spring units the yawing and rolling flexibilities are almost entirely in the forward spring, and this makes K_2 roughly $-\frac{1}{2}$. The sideslip flexibility is chiefly in the aft spring, and this makes the value of K_1 small.

Appendix B

EXPLANATION OF NEGATIVELY DAMPED SIDESLIPPING MODE

In the tests with the spring unit modified to give lower natural frequencies in roll, the sideslipping mode became negatively damped at values of the incidence above about 8°. The basic mechanism can be described as follows, an essential feature being that the natural frequency in roll had been made lower than the natural frequency in sideslip (Table 2). In the sideslipping mode, a positive sideslipping velocity causes a negative rolling moment since ℓ_v is negative (Figs.20 and 21). However, this rolling moment is applied at a frequency higher than the natural frequency in roll and as a result the model displacement in roll is in opposite phase to the rolling moment and is therefore in phase with the sideslipping velocity. The sideways component (due to this roll displacement) of the upward normal force* is then also in phase with the sideslipping velocity and thus provides a negative contribution to the damping of this mode. This contribution increases with incidence because both ℓ_v and the normal force increase with incidence. The ordinary sideslip damping is positive (y_v is negative) and substantially independent of incidence (Figs.17 and 18). The result is that the overall damping becomes negative at values of the incidence above about 8°.

The oscillation was controlled by applying artificial damping by means of a feedback amplifier which forms part of the standard equipment used for these tests, and in principle the derivatives obtained are independent of the modes of oscillation. In practice, however, the derivatives obtained primarily from the sideslipping mode (particularly n_v and y_v) show a considerably increased scatter when the overall damping was negative.

---

* The relevant derivative is actually the uncorrected y_ϕ shown in Fig.22 which is not exactly equal to the normal force.

Appendix C

ANALYSIS OF CALIBRATIONS

The first stage of the calibration procedure is to make a series of measurements with a special calibrating frame instead of the model, making systematic changes in the various inertias. From the values of resonance frequencies and accelerometer signal ratios it is then possible to calculate the stiffnesses of the spring unit, the inertias of the calibrating frame, and the accelerometer constants. The method is described in Appendix B of Ref.1, but the calculations are somewhat tedious, and cannot be done easily by a computer because there is a considerable amount of redundant information which has been deliberately retained in order to check that the system conforms to the assumed equations of motion.

We have found it better to use a trial and error method of determining these constants, that is to say to assume a set of preliminary values of stiffnesses and accelerometer constants and to use these to calculate the inertias for each of the conditions tested. (These calculations are done by computer.) It is then easy to check whether the changes of inertia calculated in this way agree with the changes actually made, and, if not, to modify the values of the constants for a second attempt. A further check is obtained from the fact that each cross inertia can be obtained in two different ways. The mass moment $m\,\bar{x}$, for instance, can be obtained independently from the yawing moment and the side force equations, and the two values should be the same. In practice, the effects of changing the various constants can be fairly easily separated, and only a few iterations are needed to obtain a satisfactory set of values of the constants.

The second stage of the calibration procedure is to make a series of measurements on the model over a frequency range on either side of resonance in each mode. The resonance tests give the model inertias in terms of the known stiffnesses, and the off-resonance tests are used to obtain the excitation calibration constants. Here again a trial and error method is better than calculating the constants directly from the readings, and the criterion is that there should be no change in any stiffness with frequency.

These methods were adopted partly to save time and labour, but they have other advantages. When redundant information is used for determining the constants, some discrepancies are bound to occur, and the new method shows these in a much clearer form. In some cases this has indicated that additional corrections are needed, as for instance the effect of gravity on certain accelerometer readings. In other cases, when the discrepancies are caused by non-linearities or other departures from an ideal system, the results give a direct indication of the effect of such departures on the accuracy of the measurements. Finally, like most iterative processes, the method is self-checking.

Table 1

MAIN DIMENSIONS OF MODEL

Scale		1/8
Wing area	S	6.76 sq ft
Wing centre line chord	c_o	5.00 ft
Wing span	b	2.50 ft
Position of reference axis		0.548 c_o

Direction of x axis, which is also the incidence datum, is 1.5° nose down relative to wing centre line chord

Table 2

TEST CONDITIONS

Tunnel	8 ft by 8 ft				13 ft by 9 ft	
V (ft/sec)	298	211	107	105	198	137
H (in. mercury)	15	30	116	60	30	30
R (millions)	4.7	6.6	12.9	6.6	6.2	4.3
q (lb/sq ft)	52.0	52.5	53.0	26.5	47.5	22.6
Spring unit (see Fig.21)	Original				Modified	
Yawing frequency (cps)	3.4				3.3	
Sideslipping frequency (cps)	5.9				5.7	
Rolling frequency (cps)	13.4				4.9 to 6.3	
ν (yawing)	0.36	0.51	1.00	1.02	0.52	0.75
ν (sideslipping)	0.62	0.88	1.73	1.75	0.90	1.30
ν (rolling)	1.42	2.00	3.91	4.00	0.77* to 1.00	1.11* to 1.18

* See Table 4.

Table 3

SUMMARY OF RESULTS

Figs.	Derivative	Quality of measurement	Remarks
	Damping and stiffness derivatives		
4	$n_r - n_{\dot{v}} \cos \alpha$	Satisfactory	
7	$n_p + n_{\dot{v}} \sin \alpha$	Some scatter	Large effect of high ν
5	$y_r - y_{\dot{v}} \cos \alpha$	Some scatter	
8	$y_p + y_{\dot{v}} \sin \alpha$	Some scatter	Large effect of high ν
6	$\ell_r - \ell_{\dot{v}} \cos \alpha$	Satisfactory	
9	$\ell_p + \ell_{\dot{v}} \sin \alpha$	Satisfactory	
14	n_v (yaw)	Satisfactory	
15	n_v (sideslip)	Considerable scatter	No systematic discrepancy
16	$n_v \sin \alpha$ (roll)	Considerable scatter	
17	y_v (yaw)	Satisfactory	
18	y_v (sideslip)	Some scatter	No systematic discrepancy
19	$y_v \sin \alpha$ (roll)	Some scatter	
20	ℓ_v (yaw)	Satisfactory	
21	ℓ_v (sideslip)	Satisfactory	No systematic discrepancy except for effect of high ν
12a	$\ell_v \sin \alpha$ (roll)	Satisfactory	
	Apparent stiffness derivatives showing effects of virtual inertias and $\dot{v}$ derivatives		
10	n_y	Considerable scatter	Variation with ν^2 gives $n_{\ddot{y}}$ $(= n_{\dot{v}})$
10	y_y	Considerable scatter	Variation with ν^2 gives $y_{\ddot{y}}$ $(= y_{\dot{v}})$
10	ℓ_y	Considerable scatter	Variation with ν^2 gives $\ell_{\ddot{y}}$ $(= \ell_{\dot{v}})$
11	n_ψ	Some scatter	Variation with ν^2 represents $n_{\ddot{\psi}}$
12	ℓ_ϕ	Satisfactory	Variation with ν^2 represents $\ell_{\ddot{\phi}}$
	Apparent total model inertias in still air showing effects of virtual inertias		
13	I_{zz}	Some scatter	Variation with tunnel pressure gives $n_{\ddot{\psi}}$
13	m (sideslip)	Satisfactory	Variation with tunnel pressure gives $y_{\ddot{y}}$
13	I_{xx}	Satisfactory	Variation with tunnel pressure gives $\ell_{\ddot{\phi}}$

Table 4

DERIVATIVES WITH RESPECT TO ROLLING VELOCITY

Tunnel (ft)	V ft/sec	10^{-6} R	α	ν	$n_p+n_{\dot{v}}$ sin α	$y_p+y_{\dot{v}}$ sin α	$\ell_p+\ell_{\dot{v}}$ sin α
8 × 8	298	4.7	0	1.42	-0.0015	0.0100	-0.0123
			4	1.42	-0.0016	0.0256	-0.0163
			8	1.42	-0.0065	0.0269	-0.0162
			12	1.42	-0.0072	0.0222	-0.0169
			16	1.43	-0.0169	0.0590	-0.0153
			20	1.44	-0.0315	0.0759	-0.0133
	211	6.6	0	2.00	0.0002	0.0124	-0.0122
			4	2.00	-0.0024	0.0207	-0.0165
			8	2.00	-0.0034	0.0292	-0.0168
			12	2.01	-0.0035	0.0373	-0.0168
			16	2.01	-0.0116	0.0548	-0.0161
			20	2.02	-0.0183	0.0696	-0.0135
	107	12.9	0	3.91	0.0027	0.0101	-0.0118
			4	3.90	0.0017	0.0201	-0.0158
			8	3.90	0.0011	0.0232	-0.0166
			12	3.90	0.0004	0.0252	-0.0169
			16	3.91	-0.0030	0.0341	-0.0168
			20	3.91	-0.0099	0.0659	-0.0164
	105	6.6	0	4.01	0.0015	0.0126	-0.0119
			4	4.00	0.0017	0.0216	-0.0156
			8	4.00	0.0003	0.0211	-0.0165
			12	4.00	-0.0009	0.0239	-0.0169
			16	4.00	-0.0017	0.0316	-0.0171
			20	4.01	-0.0073	0.0423	-0.0162
13 × 9	198	6.2	0	0.77	-0.0009	0.0038	-0.0130
			4	0.77	-0.0024	0.0266	-0.0175
			8	0.79	-0.0037	0.0240	-0.0180
			12	0.81	-0.0091	0.0464	-0.0183
			16	0.83	-0.0149	0.0604	-0.0150
			20	0.80	-0.0143	0.0128	-0.0171
			20	1.00	-0.0260	0.0843	-0.0135
	137	4.3	0	1.11	-0.0011	0.0033	-0.0125
			4	1.12	-0.0030	0.0180	-0.0171
			8	1.13	-0.0049	0.0237	-0.0179
			12	1.14	-0.0086	0.0455	-0.0183
			16	1.15	-0.0143	0.0466	-0.0170
			20	1.18	-0.0219	0.0717	-0.0134
			20	1.18	-0.0226	0.0723	-0.0138

Table 5

STATIC MEASUREMENTS

(13ft × 9ft tunnel, R = 6.3×10^6)

α	$-C_Z$	C_m	n_v	y_v	ℓ_v
0	0.058	-0.012	0.052	-0.362	-0.014
4°	0.172	-0.019	0.048	-0.345	-0.039
8°	0.314	-0.029	0.051	-0.344	-0.072
12°	0.487	-0.038	0.056	-0.380	-0.098
16°	0.668	-0.046	0.059	-0.375	-0.122

REFERENCES

No.	Author	Title, etc.
1	J.S. Thompson R.A. Fail	Oscillatory derivative measurements on sting-mounted wind tunnel models at R.A.E., Bedford. A.R.C. 28444 R.A.E. Technical Report 66197 (1966) AGARD C.P. 17 (1966)
2	P.L. Bisgood C.O. O'Leary	Interim report on low-speed flight tests of a slender-wing research aircraft (Handley-Page HP 115). A.R.C. C.P. 838 (1963)
3	T.B. Owen	Low-speed wind-tunnel measurements of oscillatory rolling derivatives on a sharp-edged slender wing. Effects of frequency parameter and of ground. A.R.C. R & M 3617 (1968)

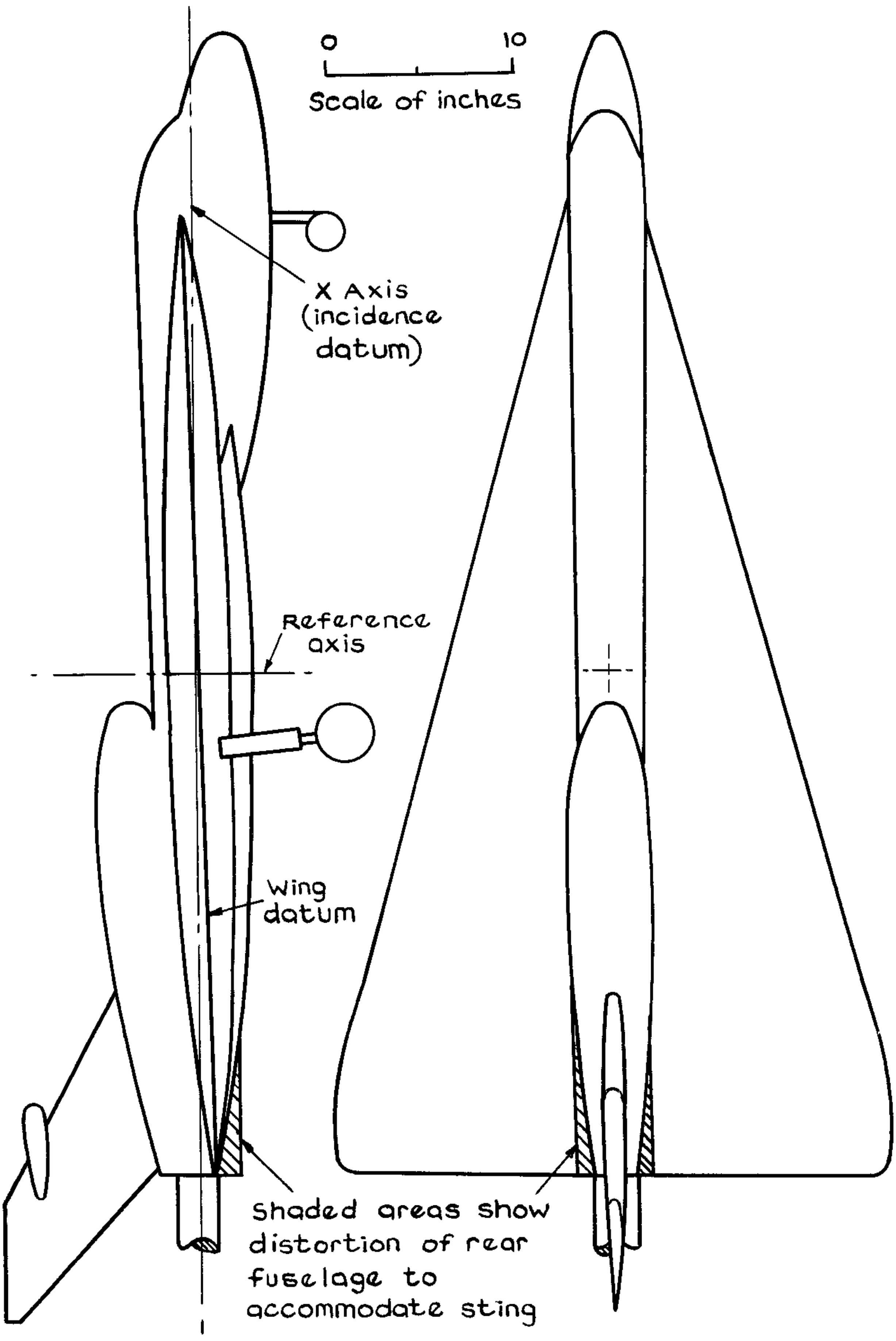

Fig. 1 Sketch of HP 115 model.

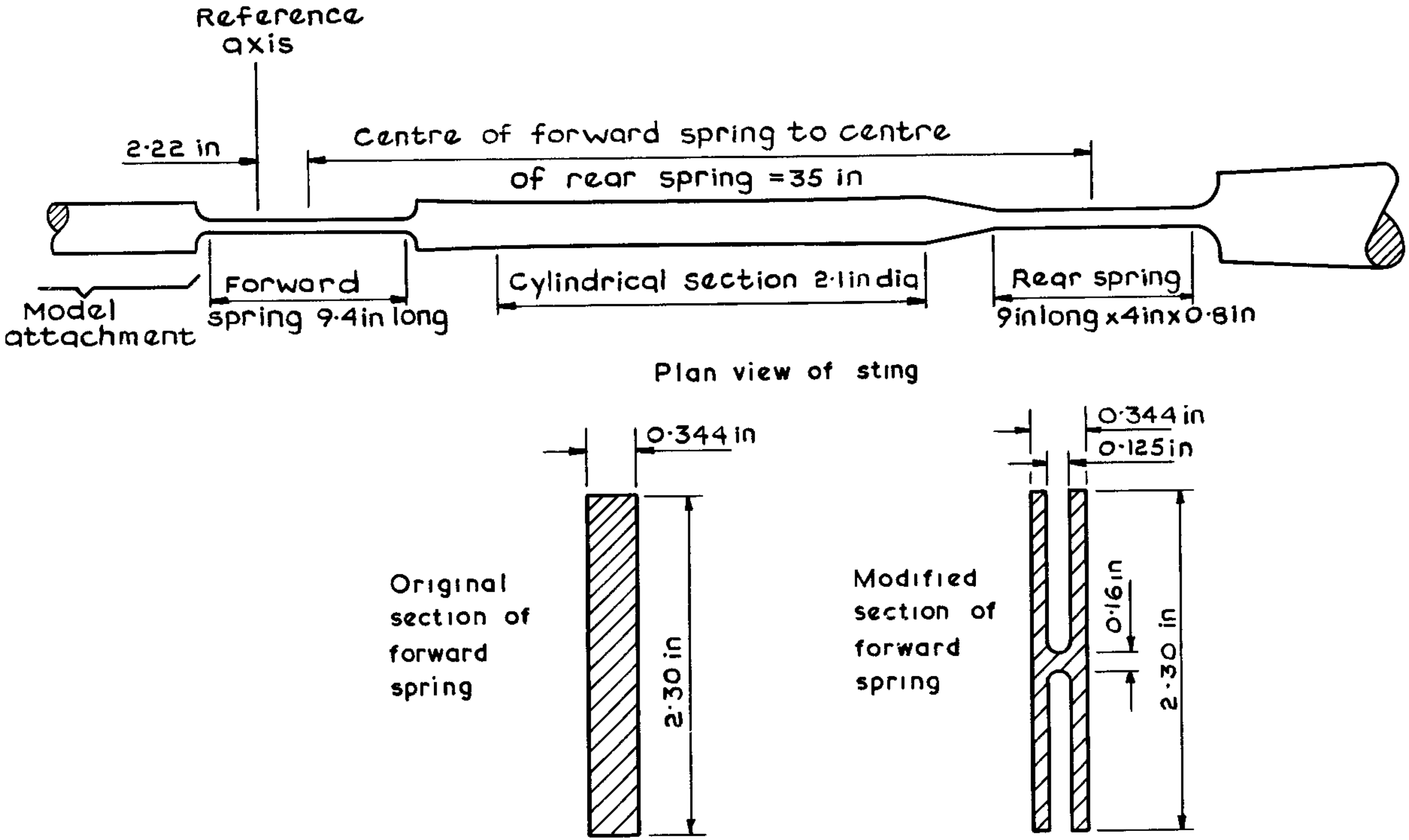

Fig. 2 Principal dimensions of spring units

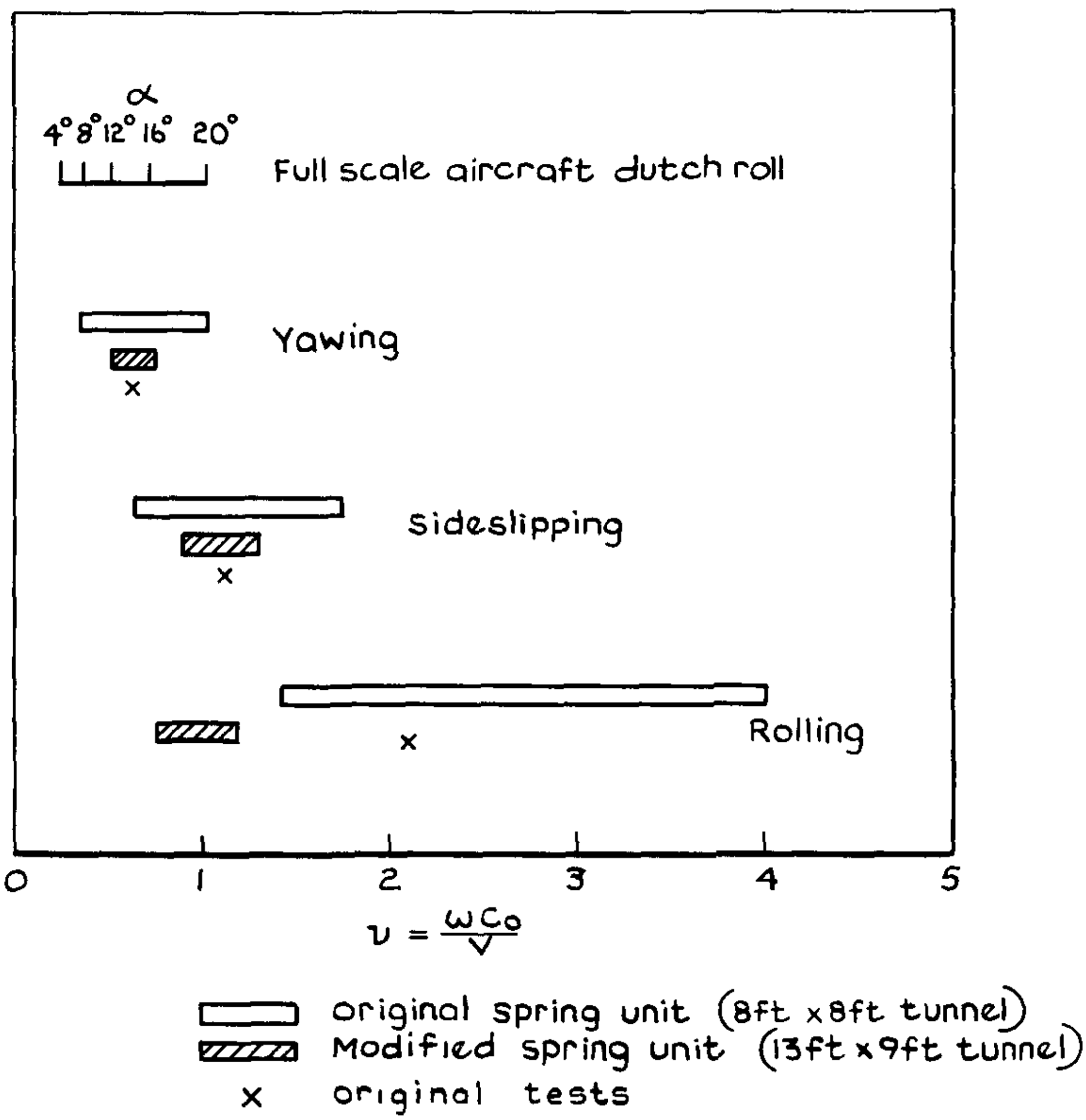

Fig.3 Ranges of test frequency parameter compared with full scale values

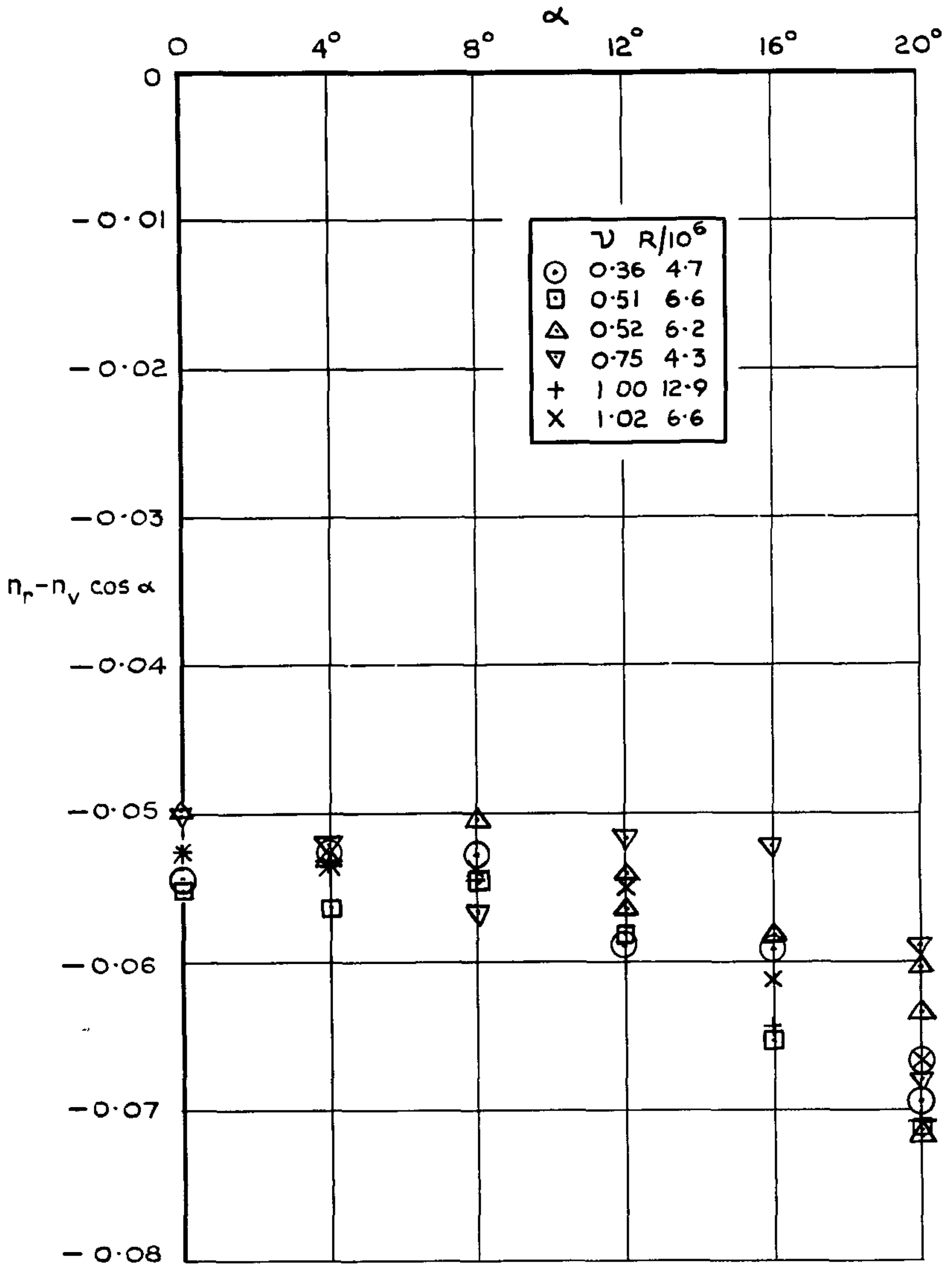

Fig.4 HP 115 yaw damping derivative, $n_r - n_v \cos\alpha$

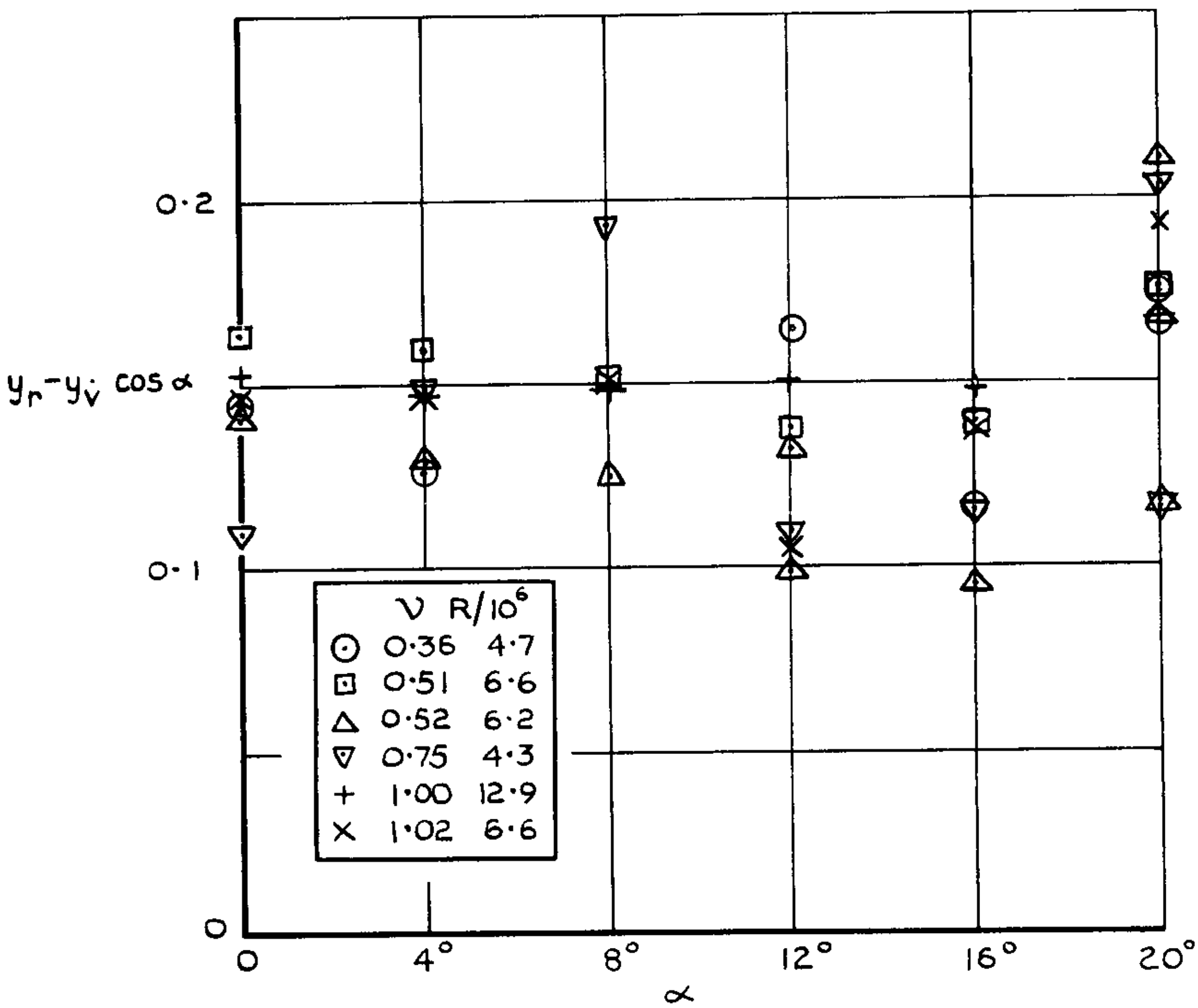

Fig.5 HP 115 cross damping derivative, $y_r - y_{\dot{v}} \cos\alpha$

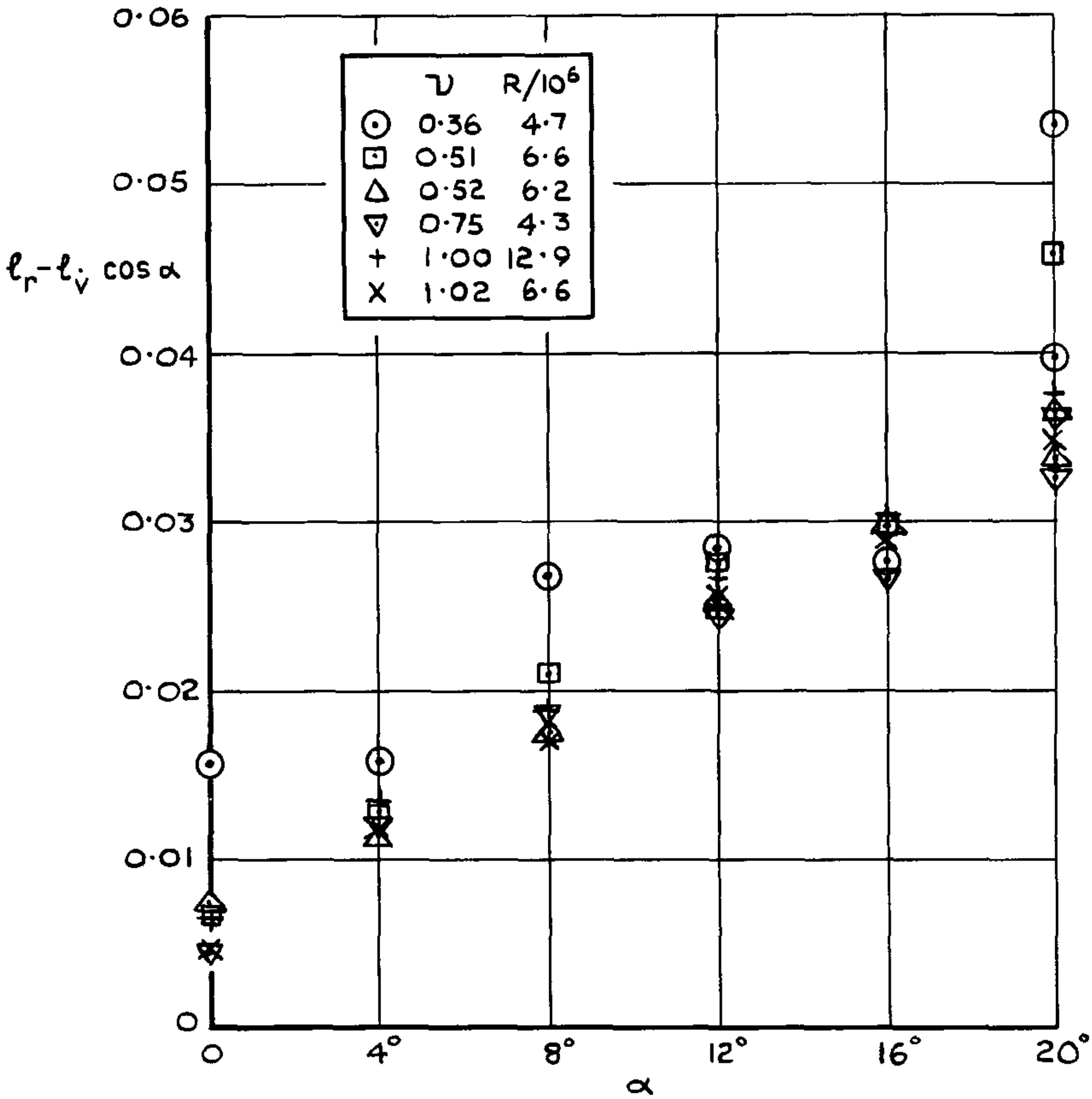

Fig. 6. HP 115 cross damping derivative, $\ell_r - \ell_{\dot v} \cos\alpha$

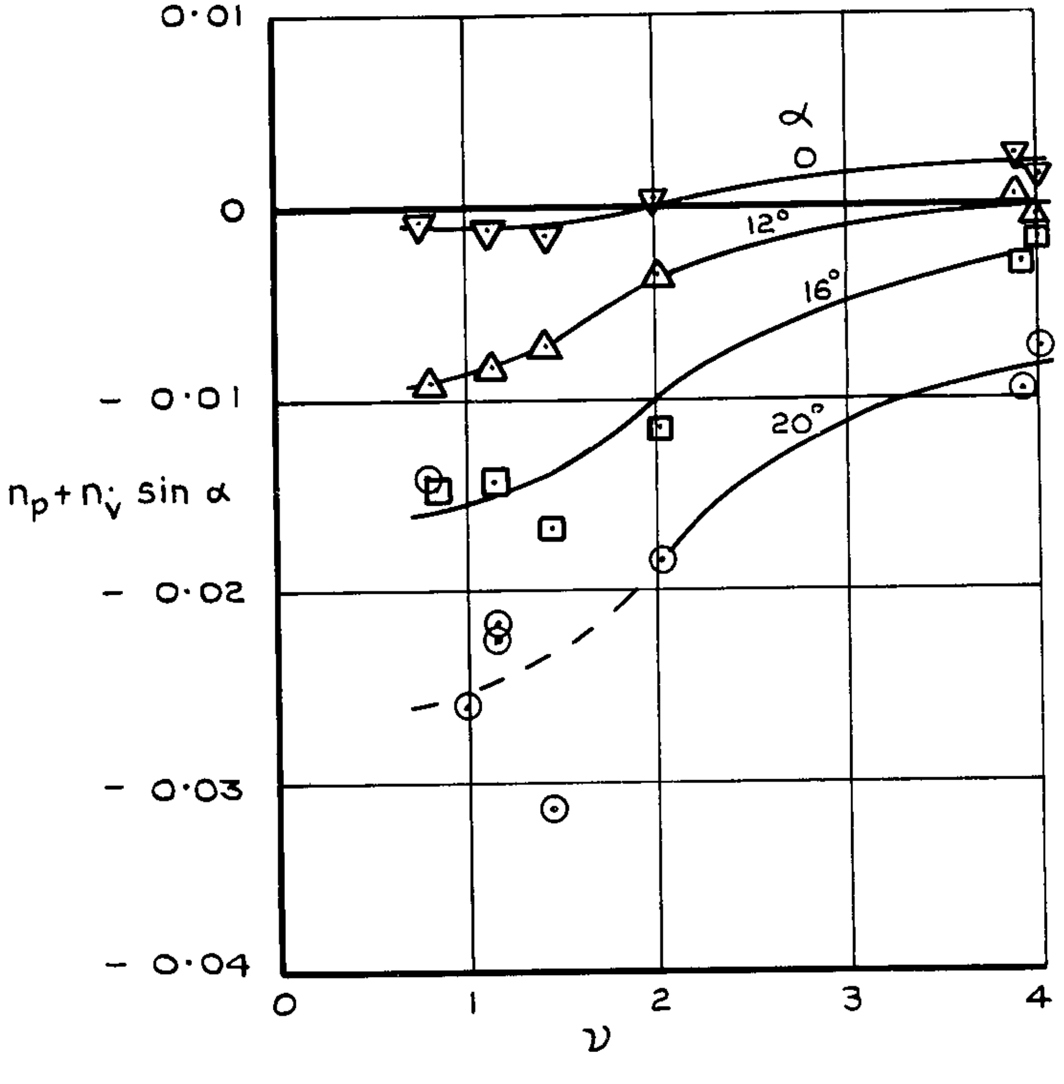

Fig. 7 HP115 cross damping derivative, $n_p + n_{\dot{v}} \sin\alpha$

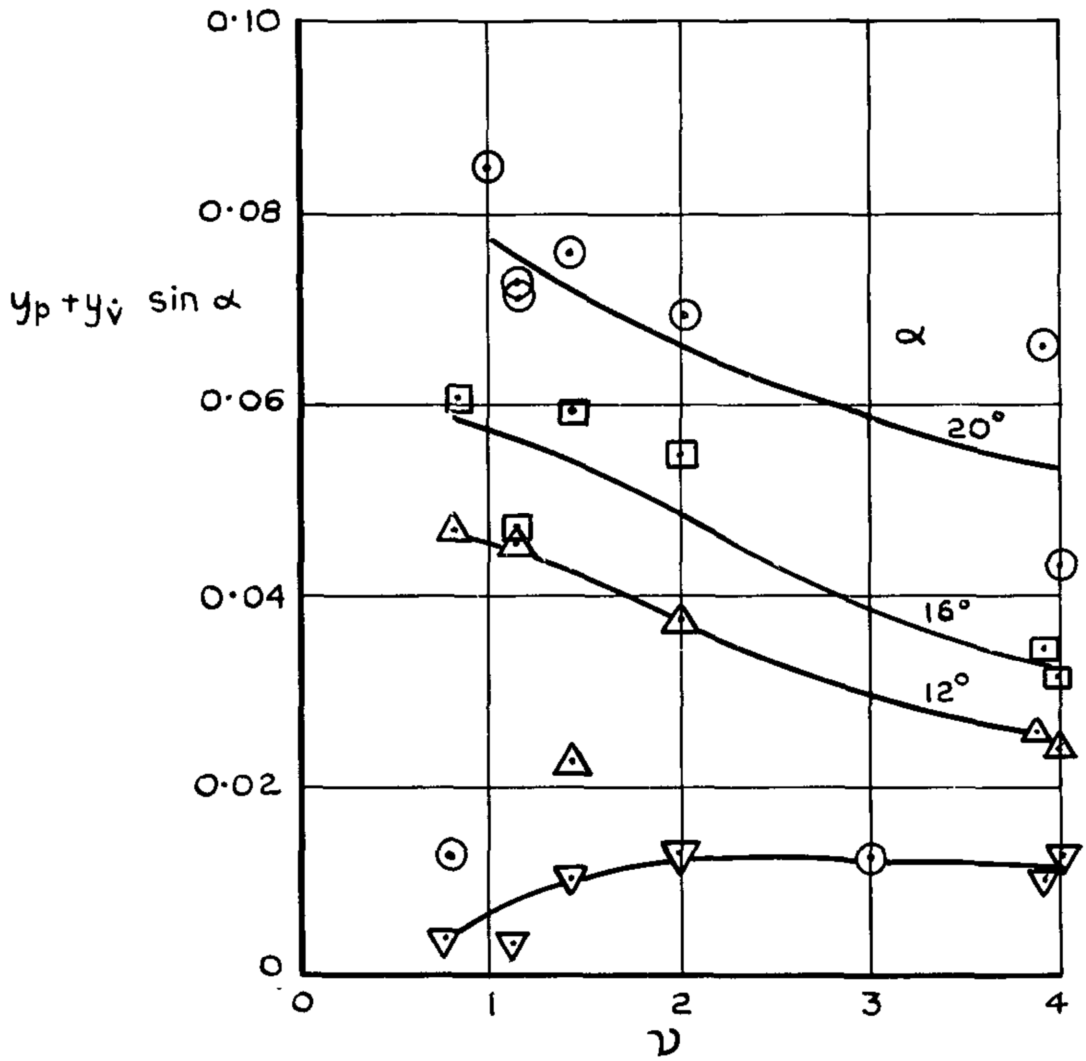

Fig. 8 HP 115 cross damping derivative, $y_p + y_{\dot{v}} \sin\alpha$

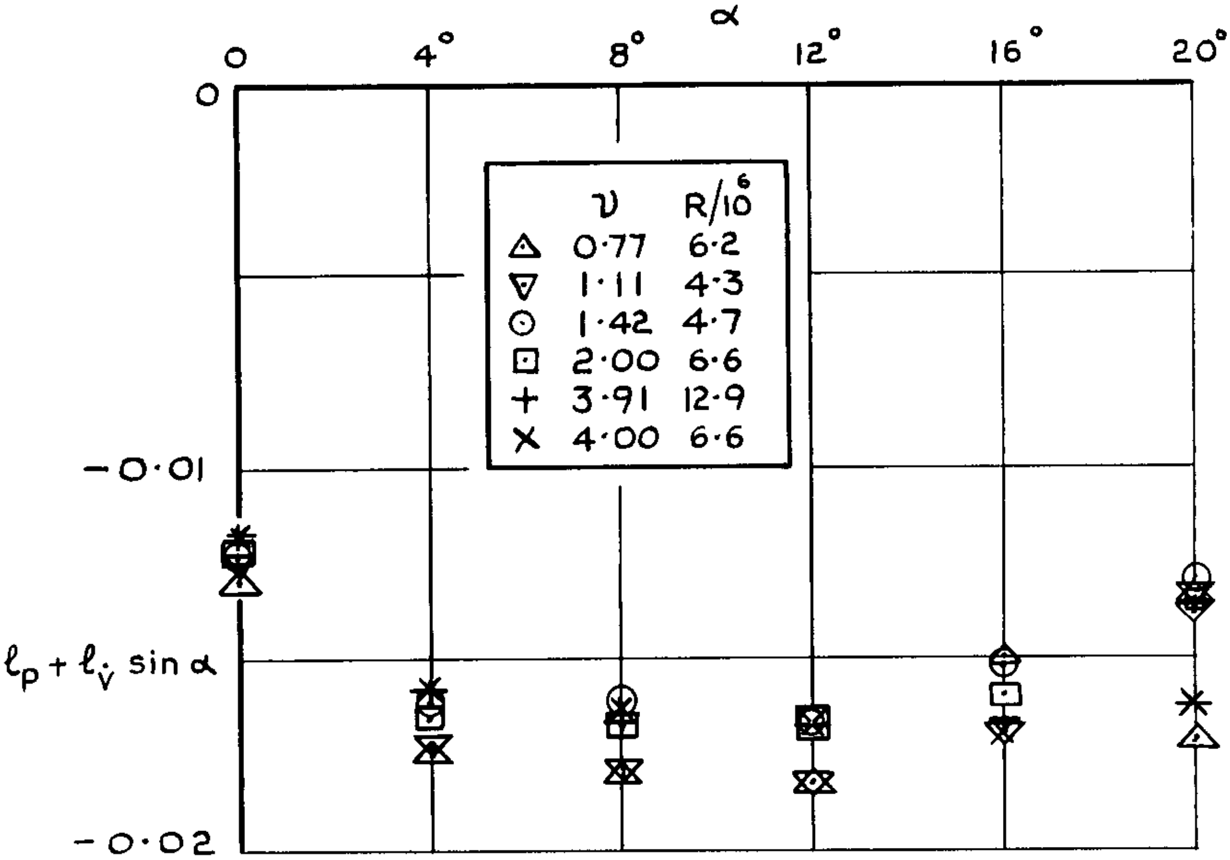

Fig 9 HP115 Roll damping derivative,
$l_p + l_{\dot v} \sin\alpha$

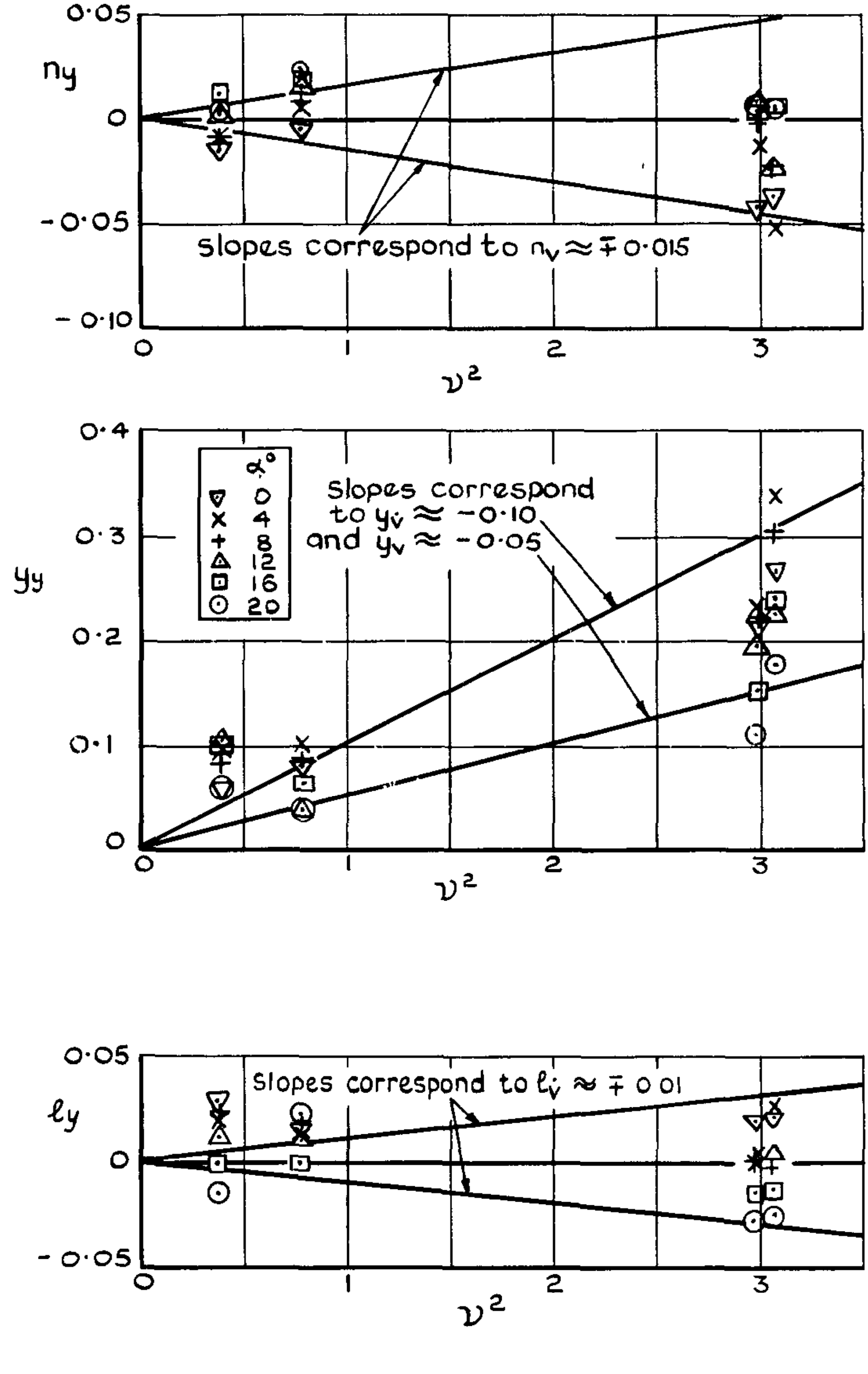

Fig 10 HP115 apparent aerodynamic stiffness derivatives n_y, y_y, and ℓ_y referred to vacuum datum

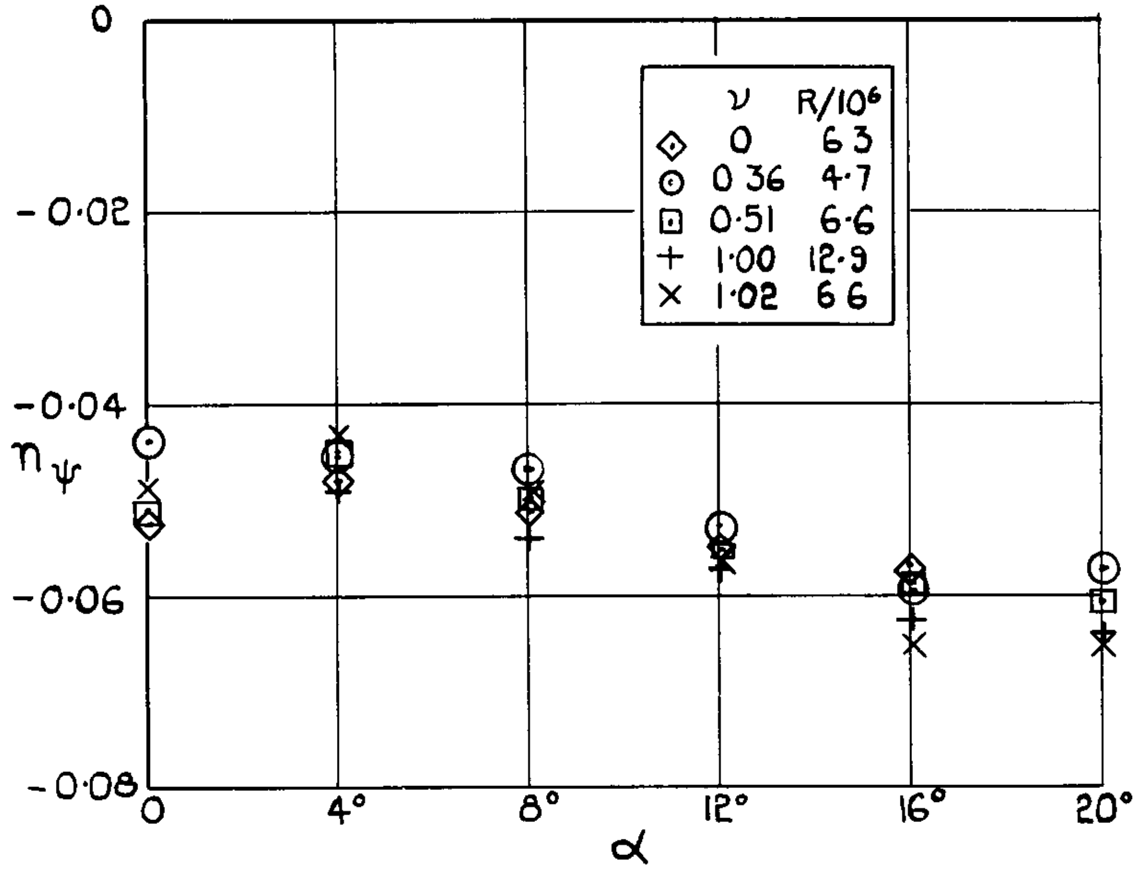

a Referred to wind-off datum at same tunnel pressure

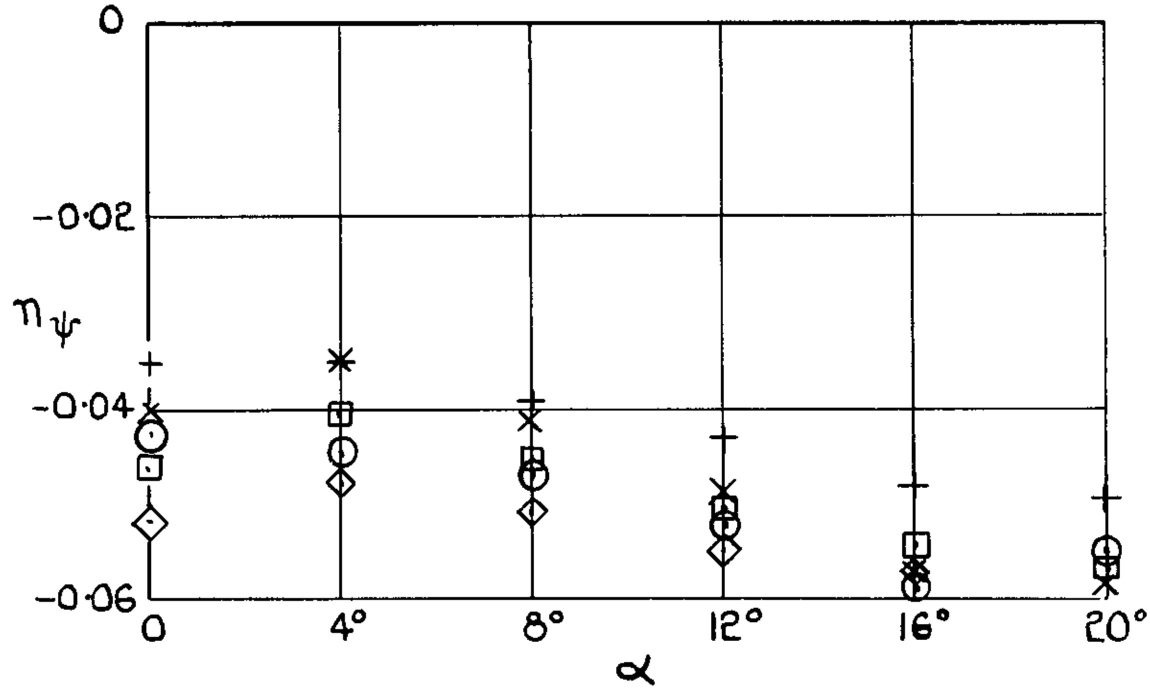

b Referred to vacuum datum

Fig 11 a&b HP 115 apparent aerodynamic stiffness derivative n_ψ

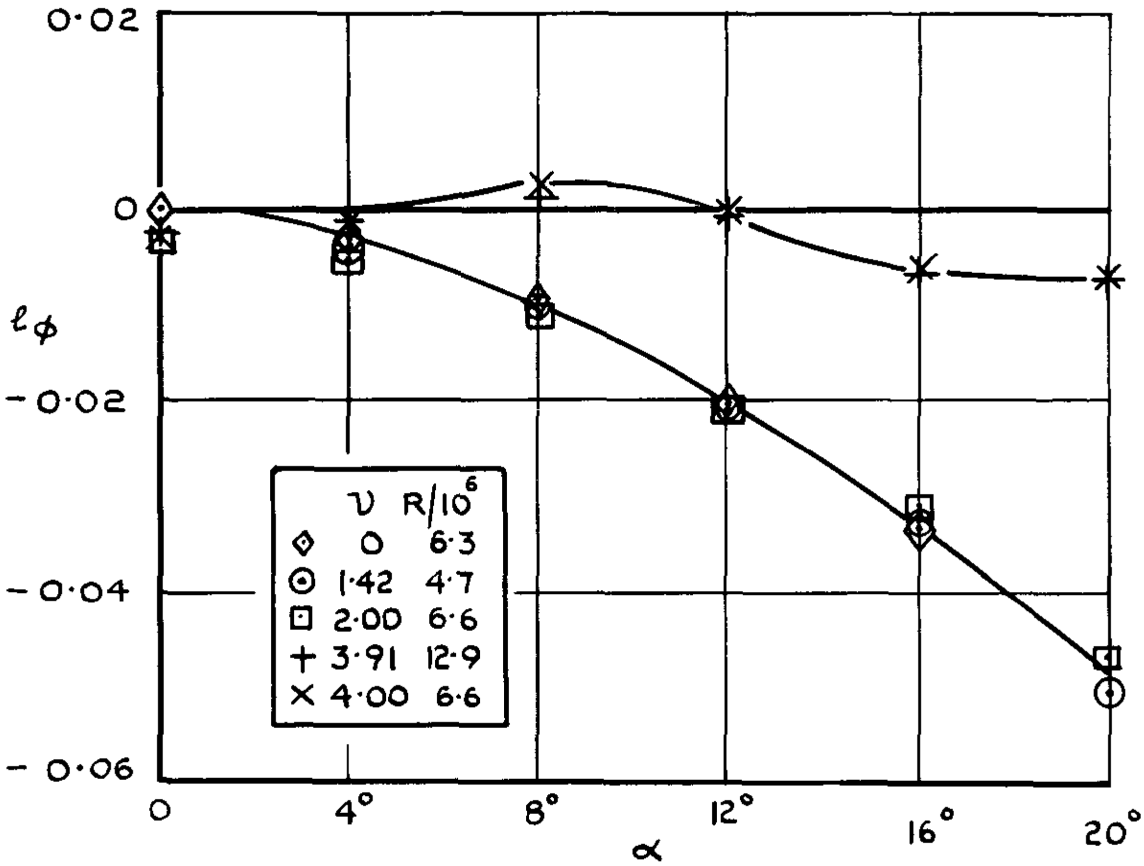

a Referred to wind-off datum at same tunnel pressure.

Fig.12a HP115 apparent aerodynamic stiffness derivative, ℓ_ϕ

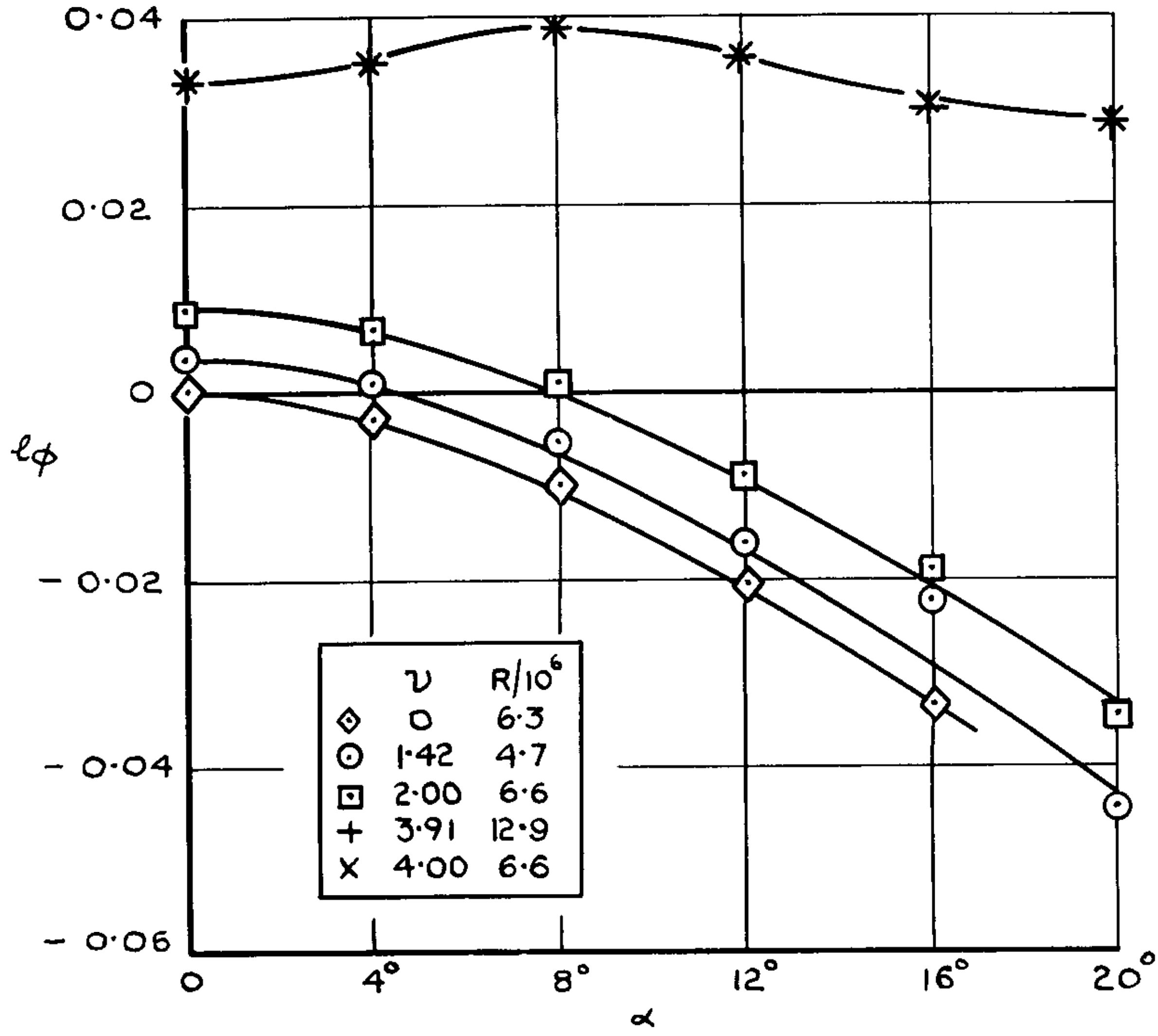

b Referred to vacuum datum

Fig. 12 contd

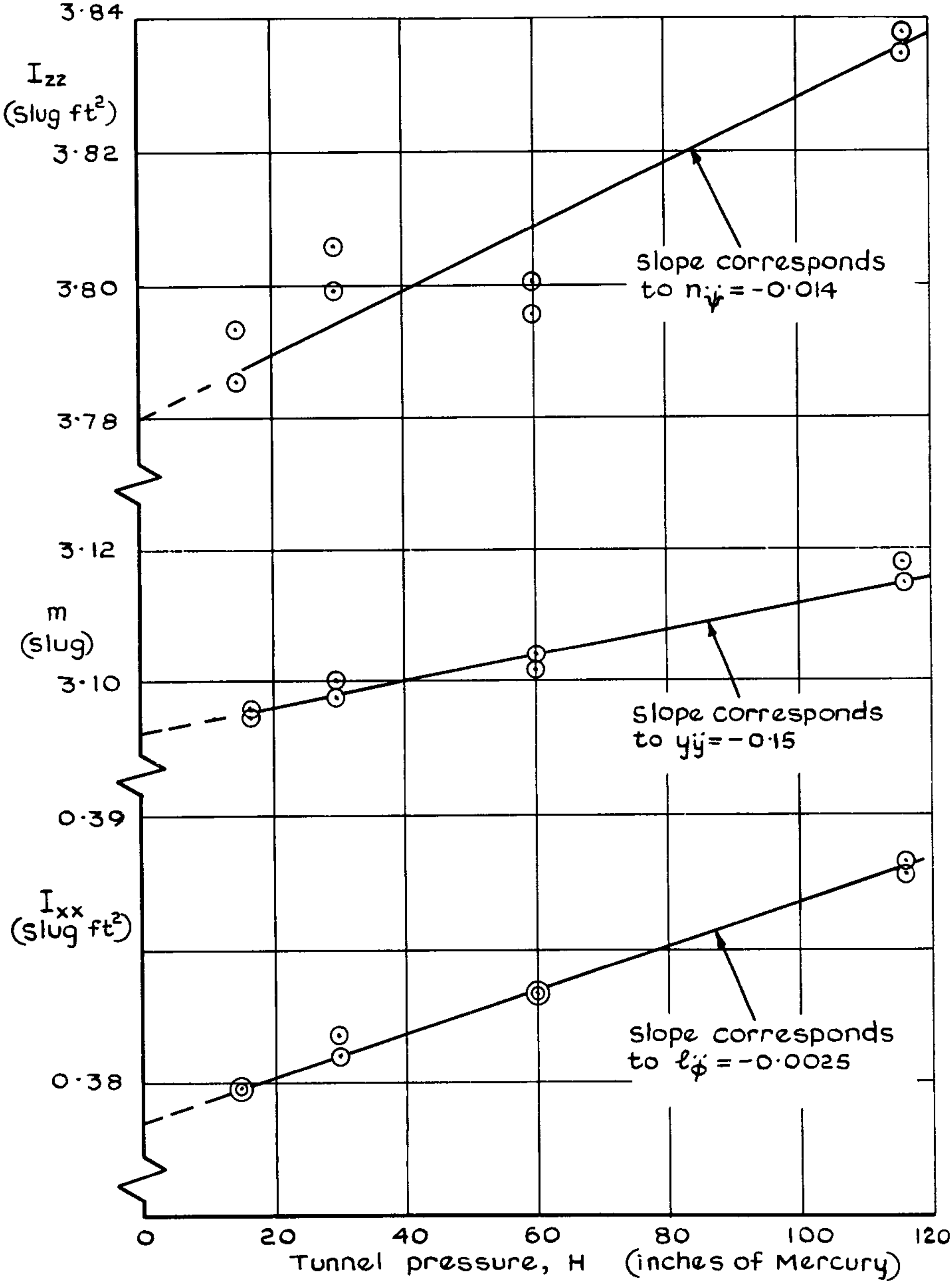

Fig 13 HP 115 Apparent total model inertias in still air (1/8 scale model)

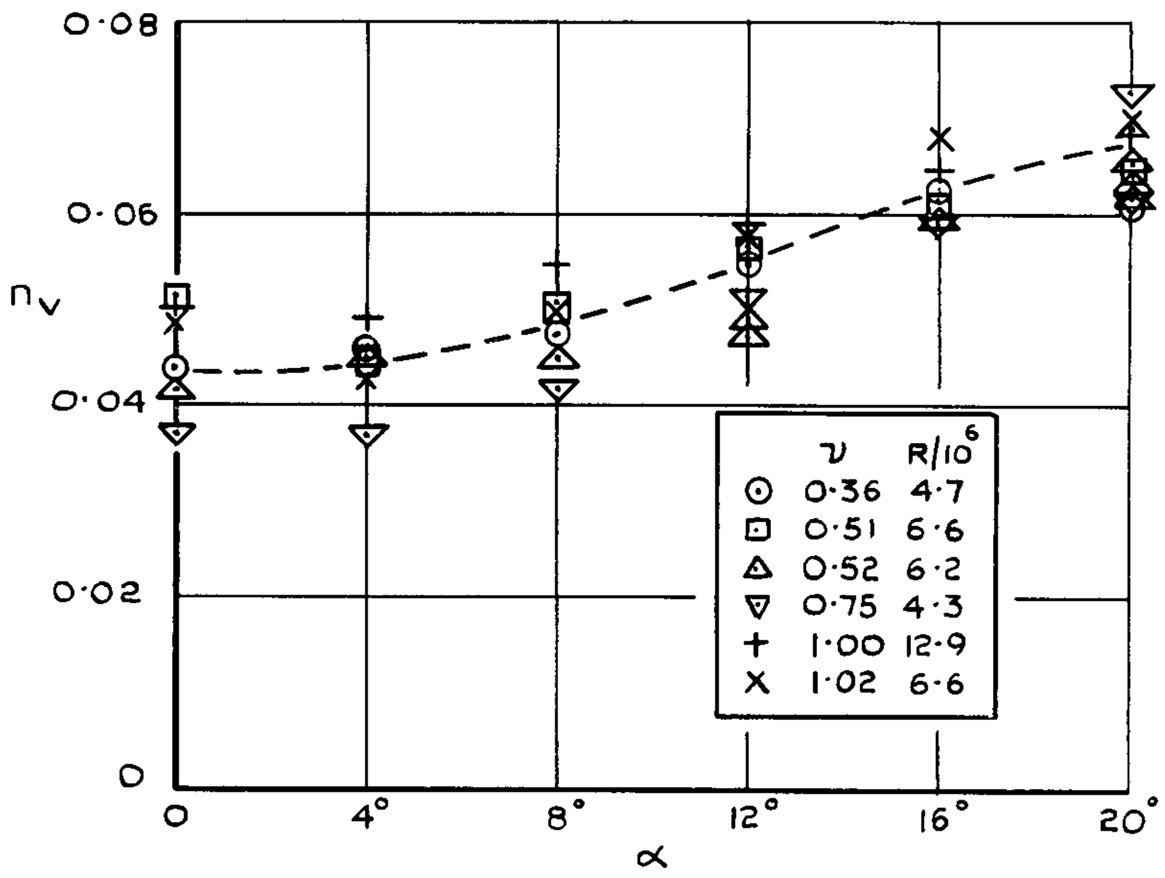

Fig 14 HP115 derivative n_v obtained from yawing motion

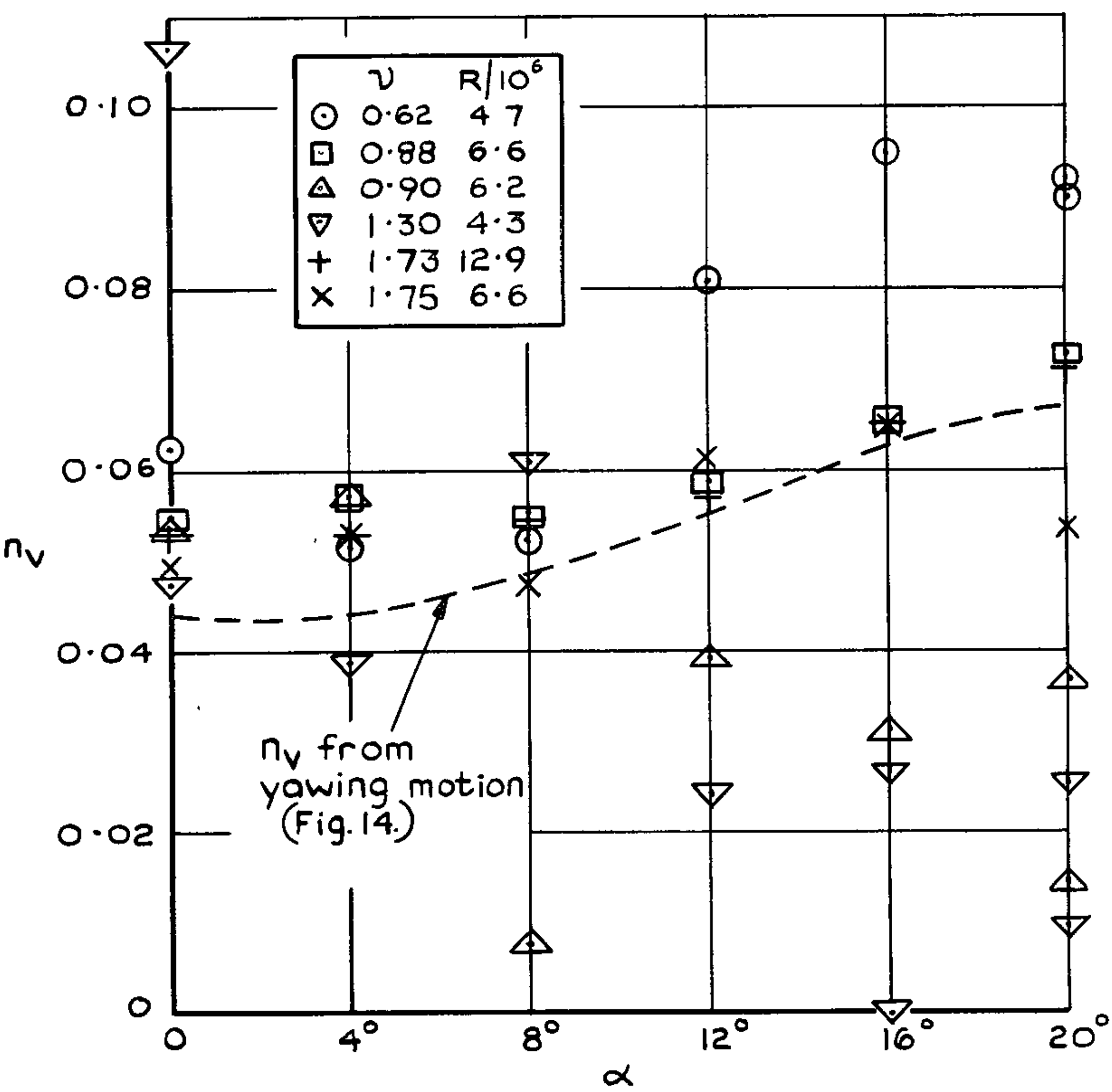

Fig 15 HP115 derivative n_v obtained from sideslipping motion

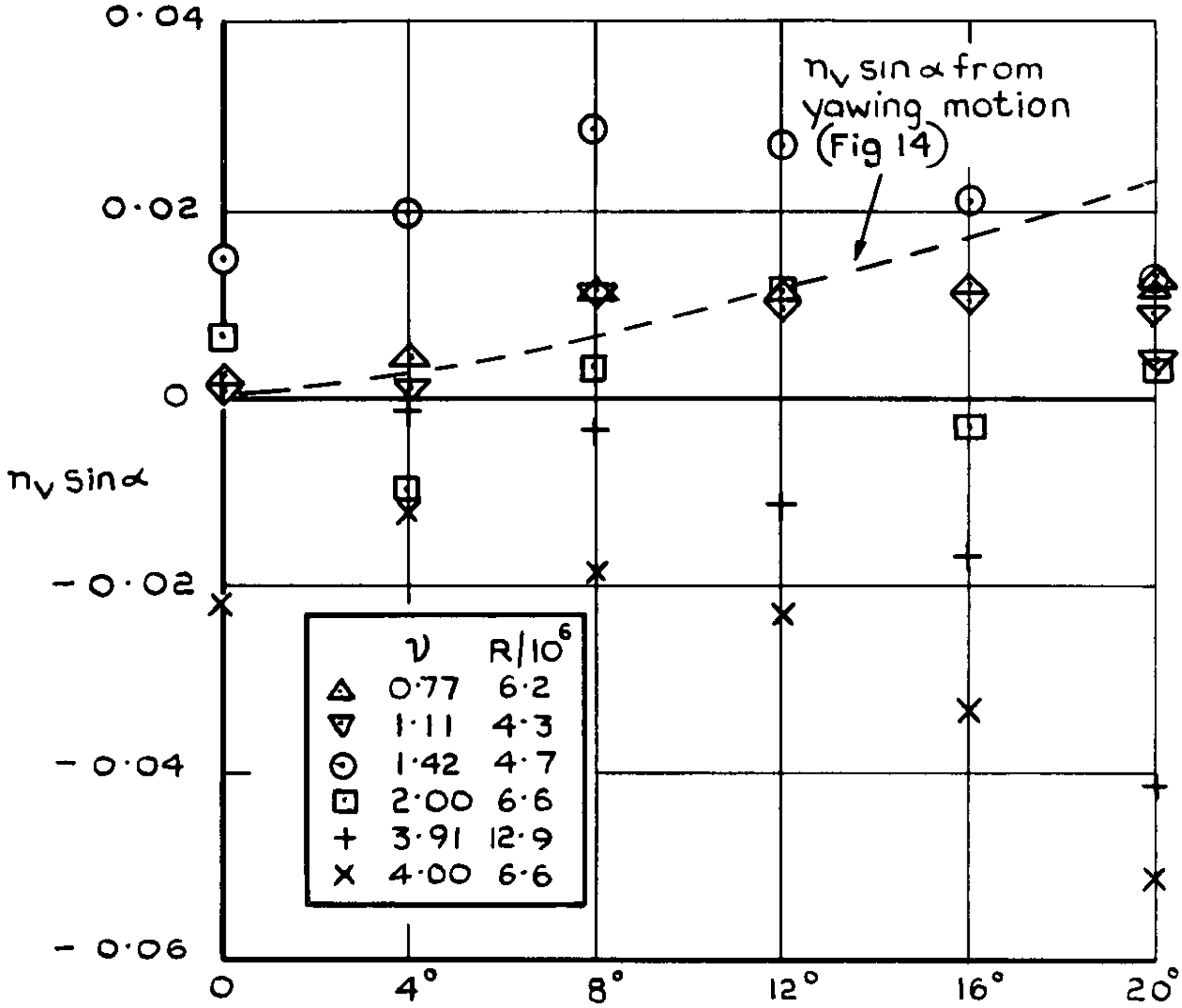

Fig.16 HP115 derivative $n_v \sin\alpha$ obtained from rolling motion

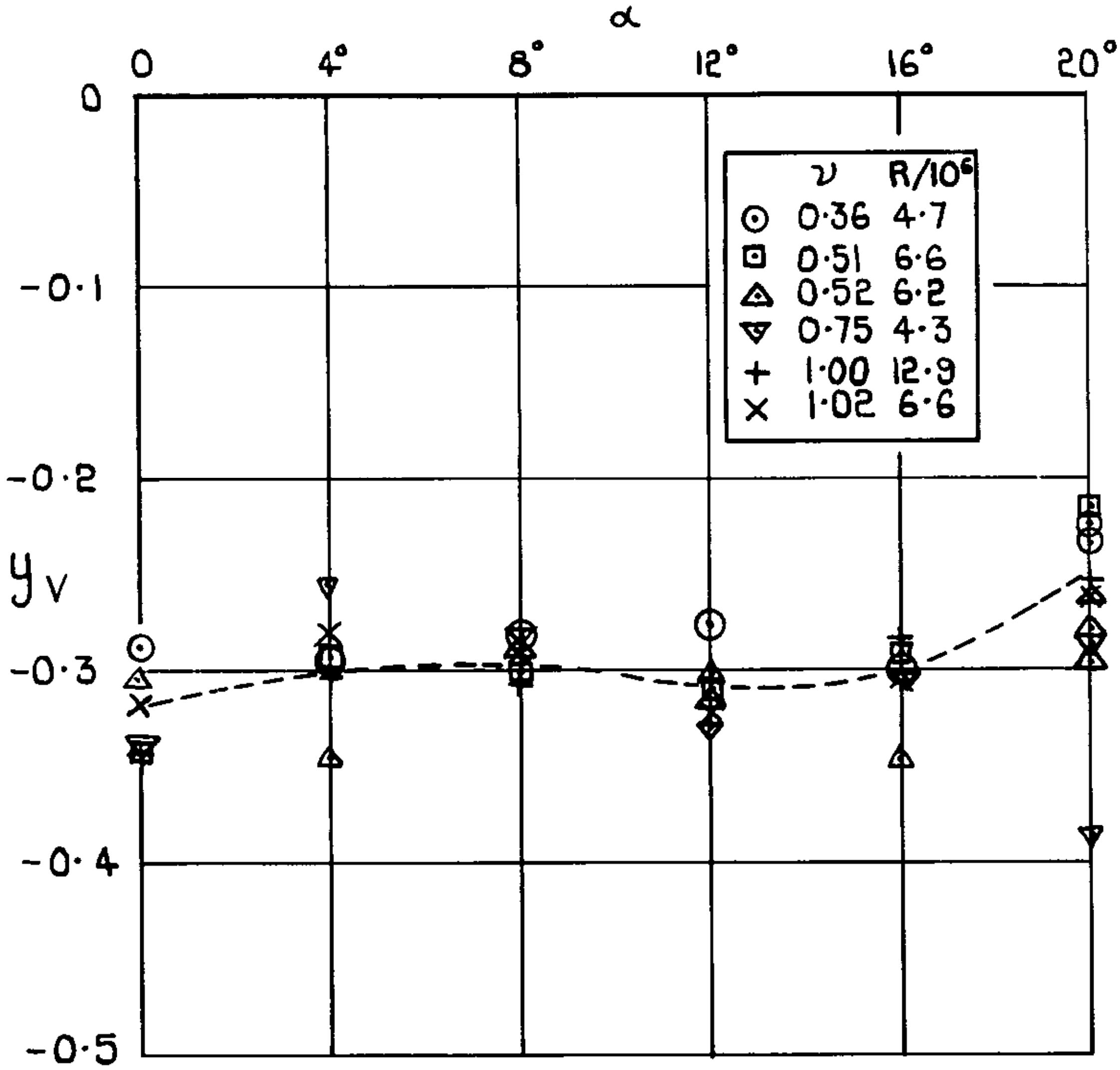

Fig 17 HP 115 derivative y_v obtained from yawing motion

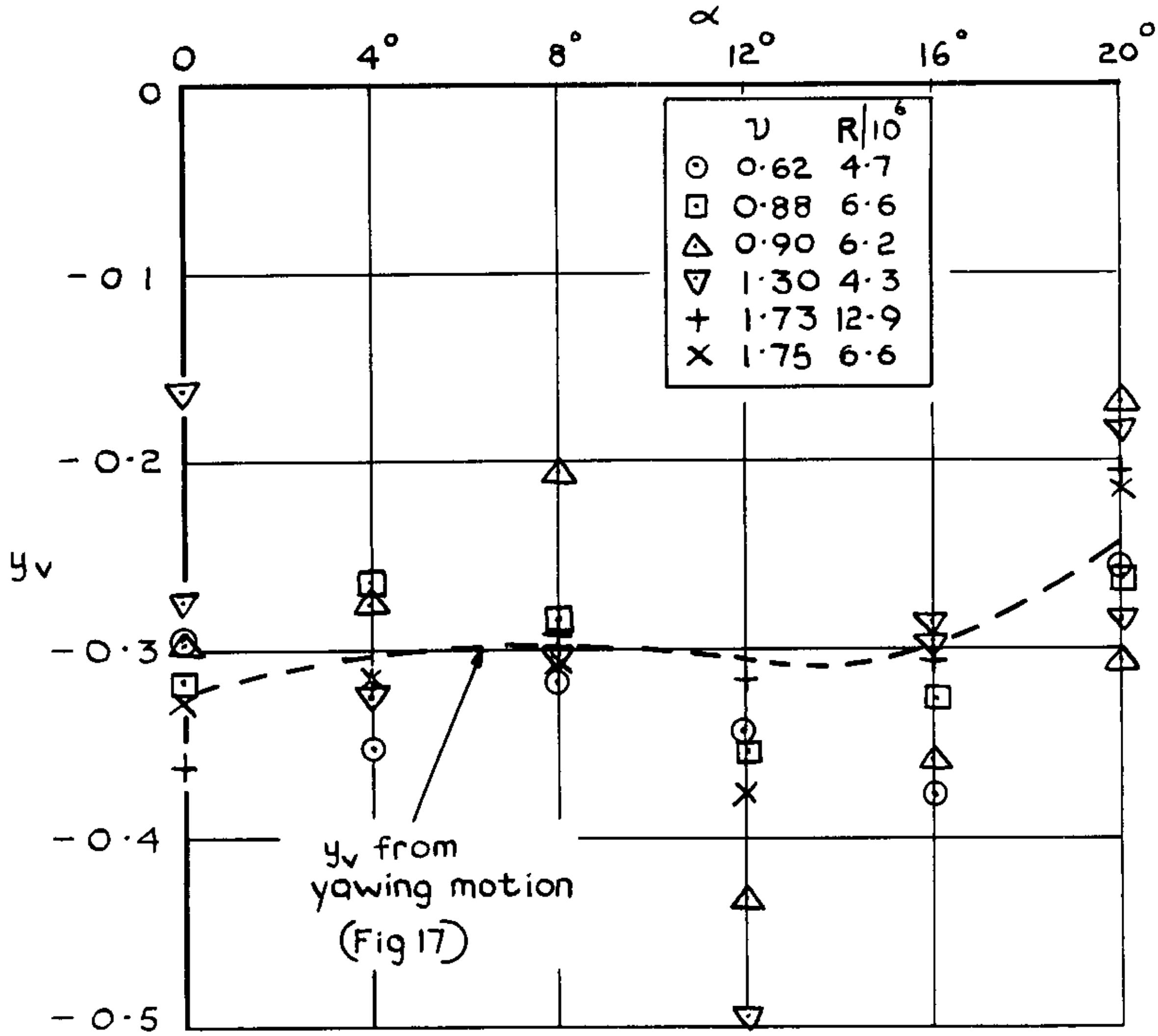

Fig.18 HP115 derivative y_v obtained from sideslipping motion

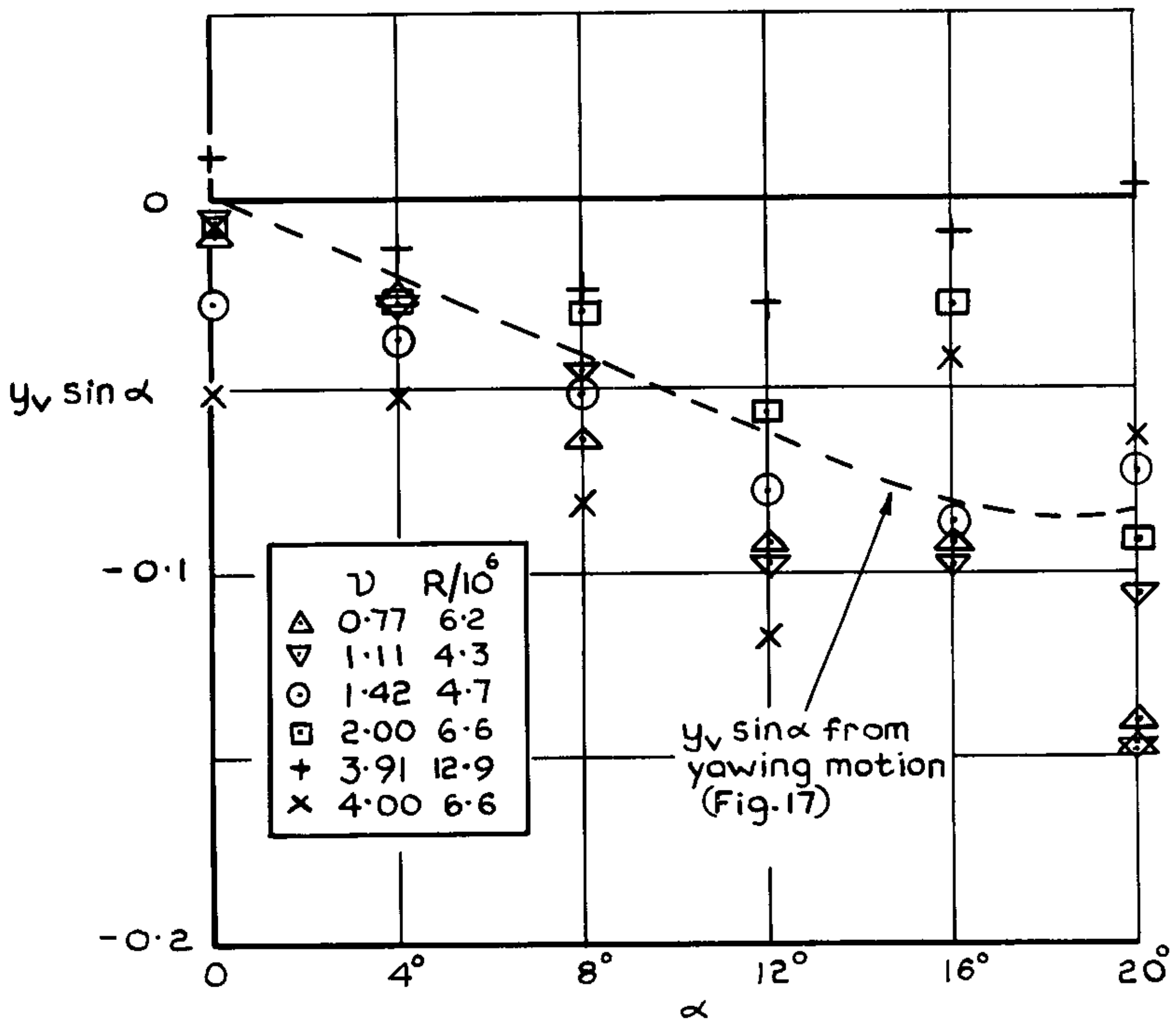

Fig. 19 HP 115 derivative $y_v \sin\alpha$ obtained from rolling motion

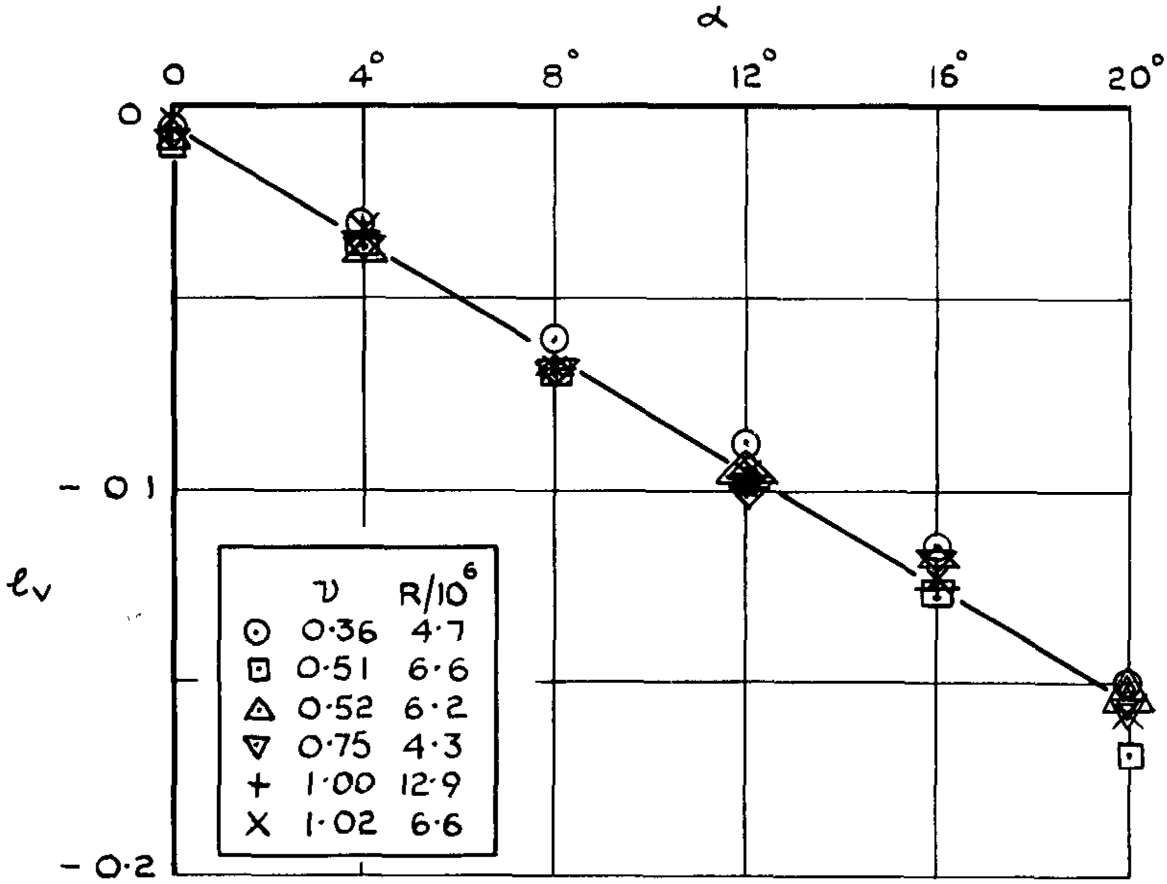

Fig 20 HP 115 derivative ℓ_v obtained from yawing motion

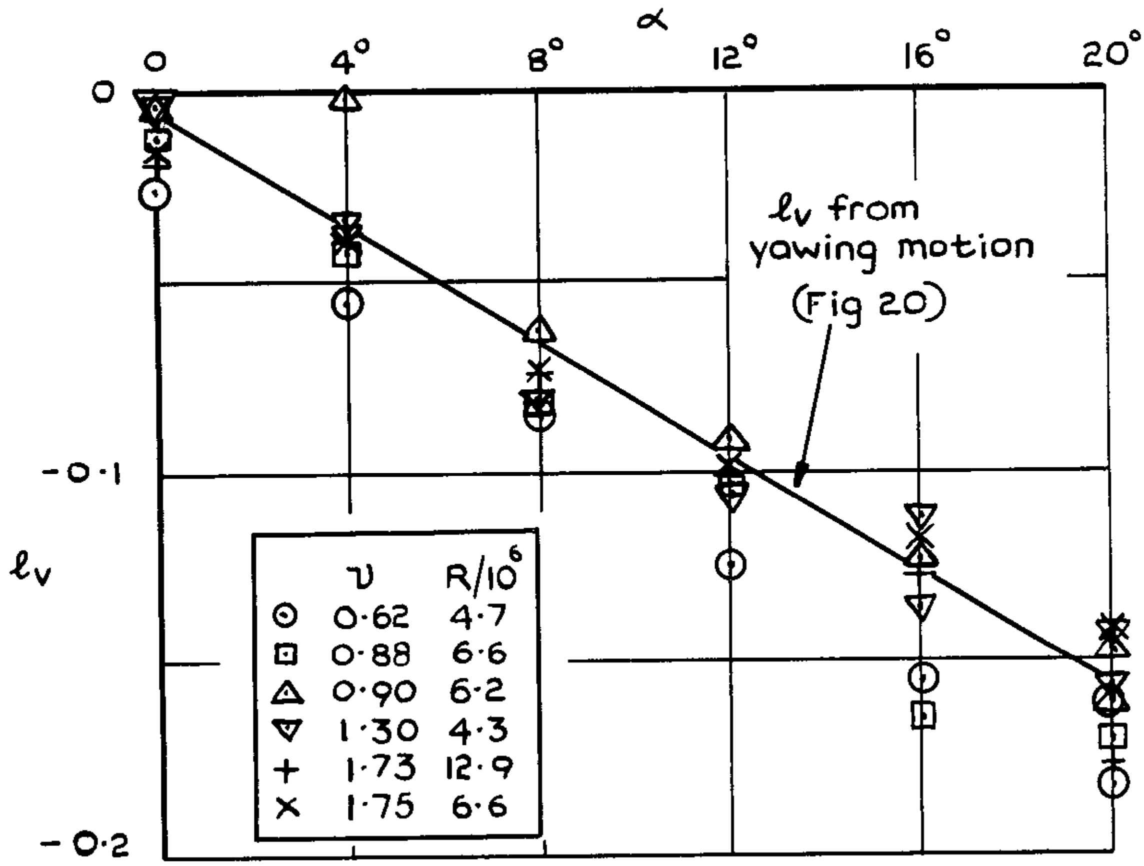

Fig.21 HP 115 derivative ℓ_v obtained from sideslipping motion

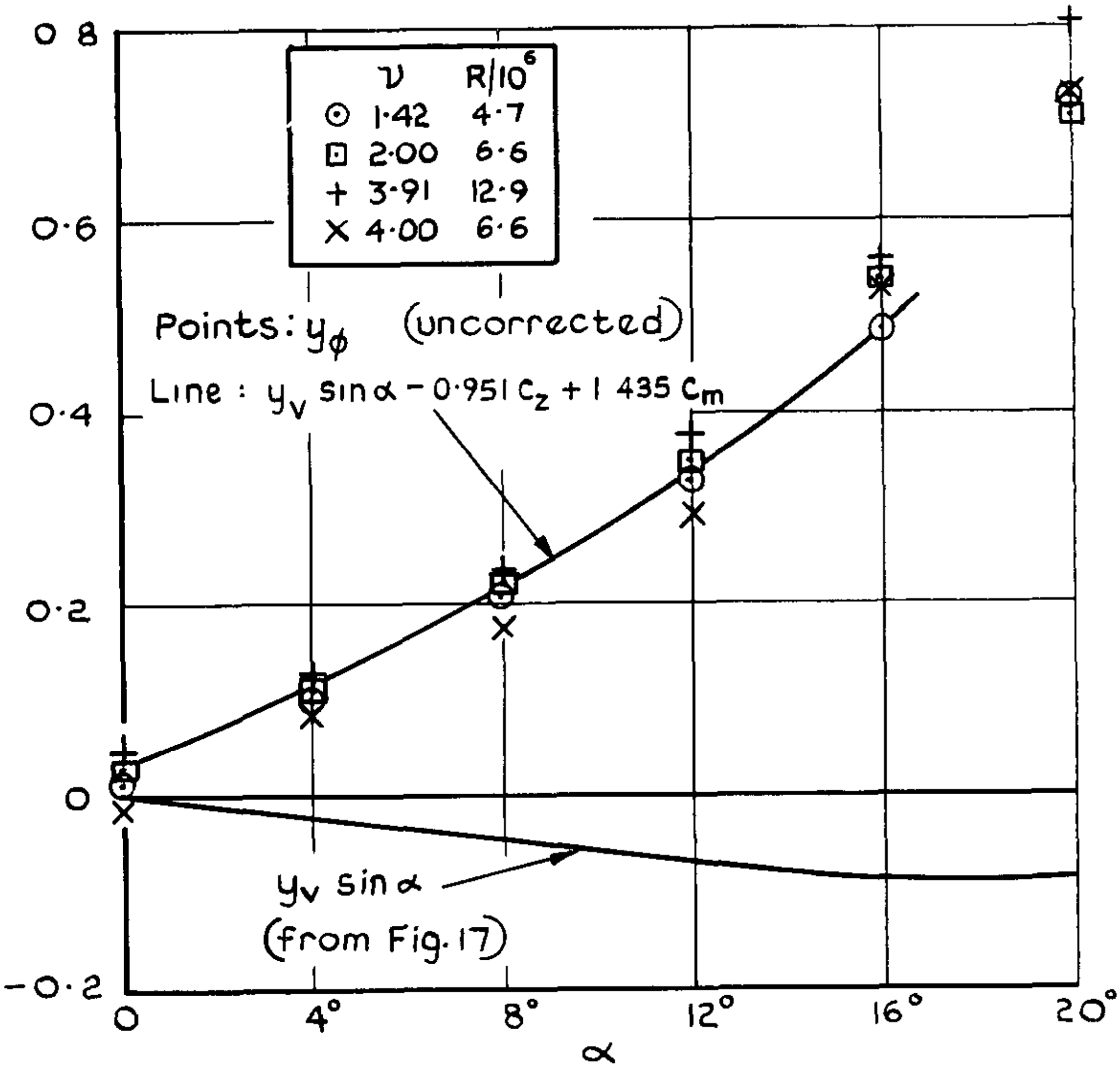

Fig. 22 HP115 values of y_ϕ showing corrections for the effects of steady loads (see sect 3)

Printed in England for Her Majesty's Stationery Office by the Royal Aircraft Establishment, Farnborough. Dd.146915. K.4.

A.R.C. C.P. No. 1097
February 1969

Thompson, J. S.
Fall, R. A.
Inglesby, J. V.

533.693.3 :
533.6.013.413 :
533.6.013.417 :
533.6.013.42

LOW-SPEED WIND-TUNNEL MEASUREMENTS OF THE OSCILLATORY LATERAL STABILITY DERIVATIVES FOR A MODEL OF A SLENDER AIRCRAFT (HP 115) INCLUDING THE EFFECTS OF FREQUENCY PARAMETER

Low-speed tunnel tests on a model of the HP 115 aircraft have provided a complete set of lateral derivatives for a range of frequency parameters. Over a range appropriate to full scale flight, the effects of frequency parameter are small, but for very high values there is a marked reduction in the derivatives n_p, y_p and ℓ_v. Some information is included on the derivatives $n_{\dot{v}}$, $y_{\dot{v}}$ and $\ell_{\dot{v}}$, and there is evidence that the virtual inertias are about the same wind-on and wind-off.

(over)

A.R.C. C.P. No. 1097
February 1969

Thompson, J. S.
Fall, R. A.
Inglesby, J. V.

533.693.3 :
533.6.013.413 :
533.6.013.417 :
533.6.013.42

LOW-SPEED WIND-TUNNEL MEASUREMENTS OF THE OSCILLATORY LATERAL STABILITY DERIVATIVES FOR A MODEL OF A SLENDER AIRCRAFT (HP 115) INCLUDING THE EFFECTS OF FREQUENCY PARAMETER

Low-speed tunnel tests on a model of the HP 115 aircraft have provided a complete set of lateral derivatives for a range of frequency parameters. Over a range appropriate to full scale flight, the effects of frequency parameter are small, but for very high values there is a marked reduction in the derivatives n_p, y_p and ℓ_v. Some information is included on the derivatives $n_{\dot{v}}$, $y_{\dot{v}}$ and $\ell_{\dot{v}}$, and there is evidence that the virtual inertias are about the same wind-on and wind-off.

(over)

A.R.C. C.P. No. 1097
February 1969

Thompson, J. S.
Fall, R. A.
Inglesby, J. V.

533.693.3 :
533.6.013.413 :
533.6.013.417 :
533.6.013.42

LOW-SPEED WIND-TUNNEL MEASUREMENTS OF THE OSCILLATORY LATERAL STABILITY DERIVATIVES FOR A MODEL OF A SLENDER AIRCRAFT (HP 115) INCLUDING THE EFFECTS OF FREQUENCY PARAMETER

Low-speed tunnel tests on a model of the HP 115 aircraft have provided a complete set of lateral derivatives for a range of frequency parameters. Over a range appropriate to full scale flight, the effects of frequency parameter are small, but for very high values there is a marked reduction in the derivatives n_p, y_p and ℓ_v. Some information is included on the derivatives $n_{\dot{v}}$, $y_{\dot{v}}$ and $\ell_{\dot{v}}$, and there is evidence that the virtual inertias are about the same wind-on and wind-off.

(over)

DETACHABLE ABSTRACT CARDS

The Paper also describes some recent improvements in technique.

The Paper also describes some recent improvements in technique.

The Paper also describes some recent improvements in technique.

C.P. No. 1097

Published by
HER MAJESTY'S STATIONERY OFFICE

To be purchased from
49 High Holborn, London w.c 1
13a Castle Street, Edinburgh EH2 3AR
109 St Mary Street, Cardiff CF1 1JW
Brazennose Street, Manchester 2
50 Fairfax Street, Bristol BS1 3DE
258 Broad Street, Birmingham 1
7 Linenhall Street, Belfast BT2 8AY
or through any bookseller

C.P. No. 1097

SBN 11 470297 7